Coastal Marine Science 43(1): 1–25, 2020

Practical mapping methods of seagrass beds by satellite remote sensing and ground truthing

Teruhisa Komatsu[1, 2], Mazlan Hashim[3], Nurjannah Nurdin[4], Thidarat Noiraksar[5], Anchana Prathep[6], Milica Stankovic[7], Tong Phuoc Hoang Son[8], Pham Minh Thu[9], Cao Van Luong[10], Sam Wouthyzen[11], Sophany Phauk[12], Aidy M. Muslim[13], Nurul Nadiah Yahya[14], Genki Terauchi[15], Tatsuyuki Sagawa[16] and Ken-ichi Hayashizaki[17]

[1] *Atmosphere and Ocean Research Institute, the University of Tokyo*
5–1–5 Kashiwanoha, Kashiwa, Chiba 288–8564, Japan. E-mail: komatsu@aori.u-tokyo.ac.jp
[2] *Japan Fisheries Resource Conservation Association,*
1–1 Akashicho, Chuoku, Tokyo 104–0044, Japan. E-mail: komatsu@aori.u-tokyo.ac.jp
[3] *Research Institute for Sustainable Environment, University of Technology Malaysia*
81310 UTM Johor Bahru, Malaysia. E-mail: mazlanhashim@utm.my
[4] *Marine Science Department, Hasanuddin University*
Jl.Perintis Kemerdekaan km.10, Makassar, 95245, Indonesia. E-mail: nurj_din@yahoo.com
[5] *Institute of Marine Science, Burapha University*
Bangsaen, Chon Buri, 20131 Thailand. E-mail: sargassum2005@gmail.com
[6] *Faculty of Science, Prince of Songkla University, Hat Yai, Songkhla 90112, Thailand. E-mail: anchana.p@psu.ac.th*
[7] *Faculty of Science, Prince of Songkla University, Hat Yai, Songkhla 90112, Thailand. E-mail: svesemenja@gmail.com*
[8] *Institute of Oceanography, Vietnam Academy of Science and Technology*
01 Cau Da, Nha Trang, Vietnam. E-mail: tongphuochoangson@gmail.com
[9] *Institute of Oceanography, Vietnam Academy of Science and Technology*
01 Cau Da, Nha Trang, Vietnam. E-mail: phanminhthu@gmail.com
[10] *Institute of Marine Environment and Resources, Vietnam Academy of Science and Technology*
246 Da Nang, Ngo Quyen, Hai Phong, Vietnam. E-mail: caoluongimer@gmail.com
[11] *Research Center for Oceanography, Indonesian Institute of Sciences (LIPI)*
Jl. Pasir Putih I, Ancol Timur, Jakarta Utara, 11048, Indonesia. E-mail: swouthuyzen@yahoo.com
[12] *Faculty of Science, Royal University of Phnom Penh*
Khan Toul Kork, Phnom Penh, 120000 Cambodia. E-mail: phauk.sophany@rupp.edu.kh
[13] *Institute of Oceanography (INOS), Universiti Malaysia Terengganu*
21030 Kuala Terengganu, Terengganu, Malaysia. E-mail: aidy@umt.edu.my
[14] *Geoscience and Digital Earth Centre (INSTeG), 01–04–12, Ground Floor, Blok T06, Faculty of Built Environment and Surveying, Universiti Teknologi Malaysia, 81310 Johor Bahru,*
Johor Darul Ta'zim, Malaysia. E-mail: nurulnadiahy@utm.my
[15] *Northwest Pacific Action Plan (NOWPAP), Special Monitoring and Coastal Environmental Assessment Regional Activity Centre (CEARAC), 5–5 Usijimashin-machi, Toyama 930–0856 Japan. E-mail: terauchi@npec.or.jp*
[16] *Remote Sensing Technology Center of Japan*
TOKYU REIT Toranomon Bldg., 3F, 3–17–1 Toranomon, MinatoKu, Tokyo, 105–0001, Japan. E-mail: sagawa_tatsuyuki@restec.or.jp
[17] *School of Marine Biosciences, Kitasato University, Kitasato*
Minami-ku, Sagamihara, Kanagawa, 228–8555, Japan. E-mail: ken-ichi@kitasato-u.ac.jp

Received 16 March 2018; Accepted 1 November 2019

Abstract — This review introduces practical mapping methods of seagrass beds by satellite remote sensing with ground-truthing surveys. It briefly explains optics for understanding how to map the seagrass beds under the sea. Ground truth data are necessarily used in classifying bottom habitats and evaluating classification accuracies. Ground-truthing surveys are classified into direct methods such as video observation and manta tow with a camera, and indirect methods such as echosounder and sidescan sonar. Seagrass remote sensing begins with relating habitats from ground truth data to pixel values of a satellite image. Since satellite images with high spatial resolution require high precision of positions of ground truth data, ground surveyors need to use GNSSs with sub-meter precision. Image processing procedures are composed of geometric correction, conversion of digital number of an image pixel to radiance or reflectance, atmospheric and water column corrections, image classification, and validation of classification results (accuracy assessment), which are simply explained. It is recommended to use Depth invariant index of Lyzenga (1981) or Bottom Reflectance index of Sagawa et al. (2010) for compensating attenuation of light through atmosphere and water column to obtain better seagrass habitat classification results.

Key words: coastal habitat mapping, satellite remote sensing, ground truthing, seagrass, bottom reflectance index, depth invariant index, GNSS, Michibiki

1. Introduction

In coastal waters, seagrass and seaweed beds (Figs. 1 and 2) provide important ecological functions such as habitats for animals (e.g. Coles et al. 1993, Dennison et al. 1993) and plants, and stabilizing effects of environments such as buffering effect of currents and water movement, promotion of sedimentation, absorption of nutrients, production of oxygen, sediment retention, etc. (e.g. Ward et al. 1984, Jeudy de Grissac and Boudouresque 1985, Komatsu 1989, 1996, Komatsu and Yamano 2000). Therefore, they contribute to marine biodiversity and also human society through ecological services (e.g. Costanza et al. 1997). They have been destroyed due to human impacts such as direct ones such as bottom trawl and reclamation and indirect ones such as pollution through aquaculture and urban and industrial wastewaters (Komatsu 1997).

Fig. 1. Photo showing *Zostera caulescens* Miki in Funakoshi Bay, Iwate Prefecture, Japan.

In the Seto Inland Sea, fish culture such as yellowtail has been developed since 1960s. In Asia, aquaculture (e.g. shrimp and marine fish farming) has also been developed since 1970–80s (e.g. Gujja and Finger-Stich 1996, Huitric et al. 2002). Aquacultures of fish such as yellowtail and sea breams have been fed with a large quantity of baits which are excreted as feces and urine into water. Since cultured fish do not consume all fed bait, leftovers and feces become organic load to the seabed. These organic matters are decomposed by aerobic bacteria consuming oxygen in seawater. Nutrients produced from organic matters with urine promote an increase in phytoplankton and generate harmful algal blooms. In such a phytoplankton rich environment, transparency is decreased. Eventually, lower depth limits of seagrass beds become shallower and seagrass beds are shrunk. On the sea bed, sediments become anaerobic condition and muddy due to accumulation of organic matters on the seabed and consumption of oxygen by aerobic bacteria decomposing organic matters. While repeats of fish culture for long time, feces, urine and leftovers of fish deteriorate water quality and bottom sediment quality. It is called as auto-pollution. Consequently, sandy bottom is changed to soft muddy bottom due to increase in thickness of anaerobic layer. The soft muddy bottom prevents seagrasses from rooting because they are easily taken off from the bottom by the waves and

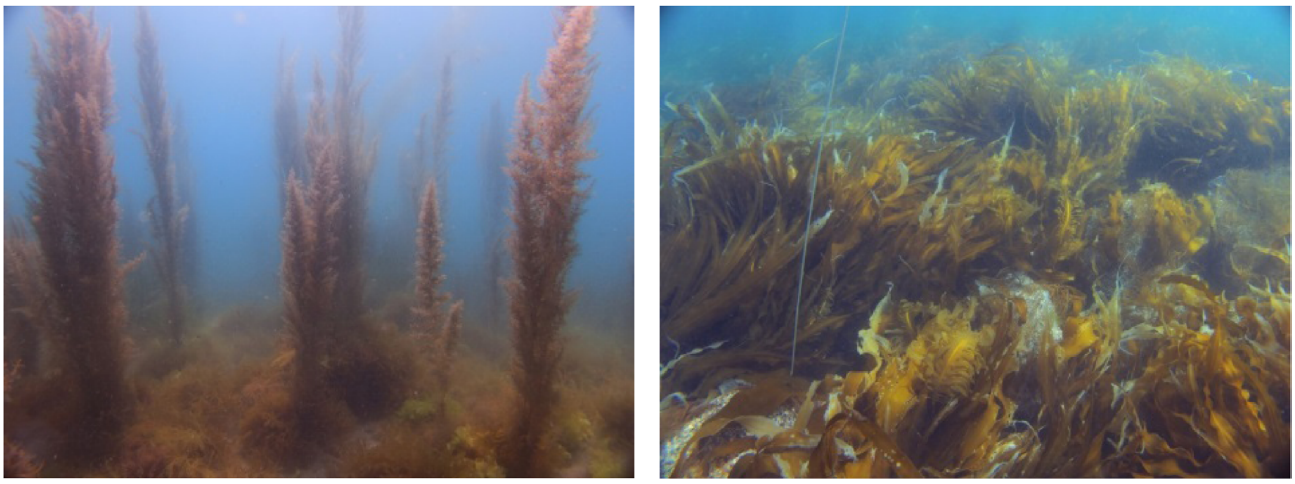

Fig. 2. Photos showing forests of brown algae, *Stephanocystis hakodatensis* (Yendo) Draisma, Ballesteros, Rousseau et Thibaut (left photo), and *Saccharina japonica* (Areschoug) Lane, Mayes, Druehl et Saunders var. *religiosa* (Miyabe) Yotsukura, Kawashima, Kawai, Abe et Druehl (right photo) off Kamoenai, west coast of Hokkaido, Japan.

currents. This is also true for waters where shrimp culture is developed because discharge from shrimp ponds causes eutrophication and lead to destruction of seagrass and seaweed beds due to water quality deterioration (e.g. Dierberg and Kiattisimkul 1996, Naylor et al. 2000) although seagrass and seaweed harbor growth-inhibiting bacteria against dinoflagellates forming red tide (Onishi et al. 2014).

Seagrass and seaweed beds, however, have to be conserved for marine biological diversity and sustainable development of fisheries and society. For maintaining sound seagrass and seaweed beds, it is necessary to map and monitor their present spatial distributions (Komatsu et al. 2001, 2012), and to establish databases and information networks to share and disseminate their data to manage these beds through monitoring them (e.g. Kirkman 1996, Komatsu et al. 2002b). We can also analyze archived satellite images to know past seagrass and seaweed distributions. Satellite remote sensing studies on seagrass beds have been conducted since mid-1980s with increase in spatial resolution of satellite imagery such as LANDSAT TM with 30 m (e.g. Haddad and Harris 1985) and SPOT 1 with 20 m (e.g. Fredj et al. 1990). Recently, spatial resolution of satellite imagery has been improved to several meters suitable for reliable seagrass mapping. In this article, we introduce a practical satellite remote sensing method specialized for mapping seagrass beds, which also applicable to seaweed beds, including validation of satellite images by ground truthing.

2. Optics for Remote Sensing

Light is electromagnetic radiation, of which the true units are W m^{-2} sr^{-1} μm^{-1}, consisting of wide range of wave lengths. Although visible and near-infrared bands are generally available in satellite images, only visible bands can penetrate into the sea deeper than ultra-violet and near-infrared which are easily absorbed by the surface thin layer (e.g. Lee et al. 2013). Thus, visible bands are used for mapping habitats in coastal waters under the sea. In the ocean, a blue band reaches the deepest and a red band is attenuated in the shallowest depths among blue, red and green bands (Fig. 3).

Remote sensing analysis with a satellite imagery utilizes radiance of the visible bands reflected by the sea beds received by an optical onboard sensor. The radiance is defined as the radiant flux emitted, reflected, transmitted or received by a given surface, per unit solid angle per unit projected area. The passage of visible band radiation from the sun to the satellite sensor is shown as a simplified schematic diagram in Fig. 4. The visible band radiation from the sun passes two layers: atmosphere and water. In both layers, a part of light is absorbed and scattered by molecules and particulates from the sun to the sea bottom and from the sea bottom to the satellite. A part of light is also reflected by the sea

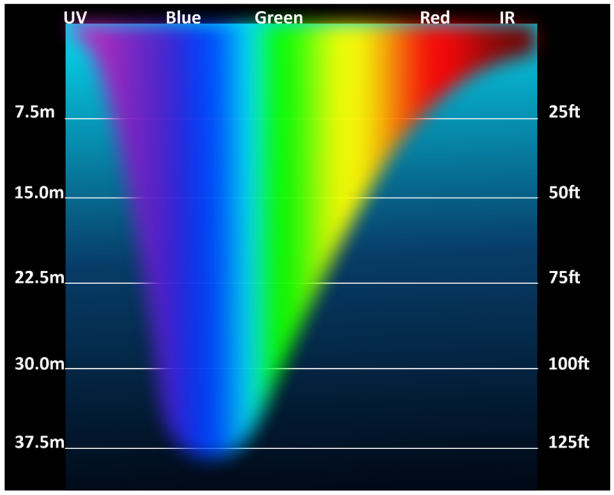

Fig. 3. Patterns of vertical penetration of light between ultraviolet and infrared into the water (courtesy of Prof. Tom Morris of Fullerton College).

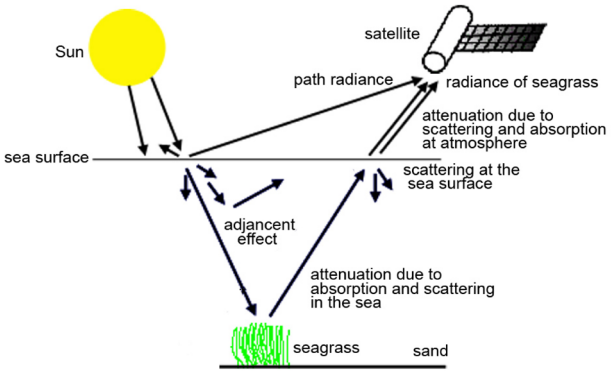

Fig. 4. Schematic view of passage of electromagnetic radiation from the Sun to the satellite sensor through atmospheric layer, sea water column and sea bottom surface.

surface. Radiances of visible bands recorded as digital numbers of pixels by the satellite sensor include bottom reflectance depending on substrate types (Fig. 4). Reflectance is a ratio of leaving to incident radiation of a certain spectral window on surface of substrate, of which reflectance depends on the bottom surface substrate types such as sand, seagrass and seaweeds. Thus, difference in reflectance of visible bands on the bottom surface under the shallow sea can be used to classify substrate types. In general, an optical sensor mounted on a satellite detects three bands of blue, green and red colors, while spectral distribution of each band depends on the optical sensor. Blue band is important to detect bottom types in deeper depth.

Figure 5 shows reflectance of sand and one species of Mediterranean seagrass, *Posidonia oceanica* L., from ultraviolet to infrared measured with a spectrometer (FieldSpec Pro, Analytical Spectral Devices Inc., USA) of which the instantaneous field of view was 25 degrees. We put samples

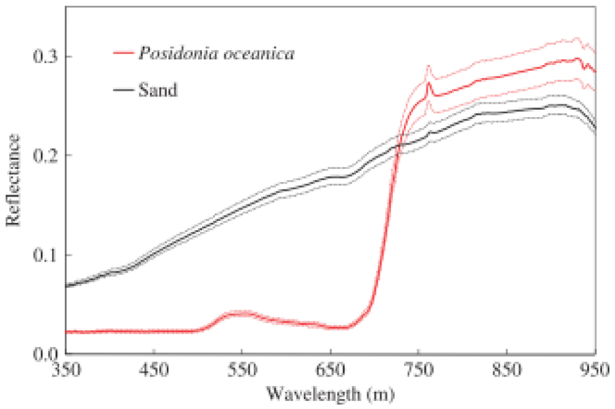

Fig. 5. Reflectance level with reference to wavelength for each bottom feature (Mahares). Values (bold lines) are shown as the mean (±standard deviation represented by broken lines). For each bottom feature, n=5 (source: Sagawa et al. 2010).

into a basin with a diameter of 30 cm, of which inside and outside were painted in black not to enter the light from surrounding environment into the basin. We measured radiances of the samples and a white disk around noon in a fine day without clouds from a wave length of 350 nm to 2500 nm at one nm intervals. Reflectance of a sample was calculated by dividing radiance of the sample with that of the white disk at each wave length. We can find the differences in reflectance of visible bands between them. Since sand reflects from short wave length to long wave length, its color is white. On the other hand, the seagrass reflects green band around 550 nm. Then its color is green. If differences in reflectance of substrate types exist corresponding to spectral windows of satellite optical sensor, it is possible to distinguish substrate types.

3. Satellite Images and Software

3.1 Spatial, spectral and radiometric resolutions of satellite images

A multiband satellite image includes multiband data which are generally composed of blue, green, red and near-infrared layers and recently adds a coastal band and red edge. Each layer consists of raster cells, pixels. One pixel corresponds to an area with intensities of upwelling radiation of the bands through the area on the Earth surface. For mapping coastal habitats, it is better that the spatial resolution of satellite images is finer than a habitat dimension to avoid a mixed pixel called as a "mixel" where different objects are close together in one pixel. For example, if two objects of brown and green exist in a pixel, its colour components of both objects result in a brown-green mixed pixel, which is hard to analyze. To map a habitat, the most important thing is that plural pixels more than five cover a patch of a habitat for detecting it. To overcome the mixel problem, it is necessary that a spatial resolution of satellite image must be quite finer than an area of a habitat. In generally, seagrass and seaweed beds are distributed in a horizontal scale of several meters to hundred or thousand meters. ALOS AVNIR-2, Geo Eye-1, IKONOS, LANDSAT ETM+, LANDSAT 8 OLI, Pleiades-1/2, Quick Bird-2, Sentinel-2, SPOT 6/7 and World View 2/3 have the spatial resolutions described in Table 1. They can detect marine habitats on the shallow sea bottom greater than their spatial resolutions. Images of GeoEye-1, IKONOS, Planet, Pleiades-1/2, Quick Bird-2 and World View 2/3/4 have very high spatial resolutions of pixel less than 4 m (Table 1).

Radiometric resolution is an ability of sensor to discriminate small differences in the magnitude of radiation within a ground area that corresponds to a single raster cell. When a bit depth (number of data bits per pixel) of images that a sensor records is great, its radiometric resolution is high. A sensor of satellite records the intensity of electromagnetic radiation from each spot viewed on the Earth's surface as a digital number (DN) for each spectral band of a pixel. The exact range of DN that a sensor utilizes depends on its radiometric resolution. The Geo Eye-1, IKONOS, QuickBird-2 and World View 2/3/4 sensors, for example, have 11 bits (0–2047) per band per pixel and LANDSAT 8 OLI, Planet, Pleiades-1/2 and Sentinel-2 have 12 bits (0–4094), while ALOS AVNIR 2 and LANDSAT ETM+ have 8 bits (0–255) (Table 1). Thus, the first two groups of satellites can distinguish small differences in the magnitude of radiation among substrate types.

Spectral resolution is the ability of a sensor to detect small differences in wavelength. A panchromatic sensor sensitive to a broad range of wavelengths has generally higher spatial resolution than those of multibands (Table 1). An object that reflects a lot of energy in the blue area of the visible band would be indistinguishable in a panchromatic photo from an object that reflected the same amount of energy in other visible bands. A sensing system with a higher spectral resolution would make it easier to distinguish the two objects apart. ALOS AVNIR 2, Geo Eye-1, IKONOS, Planet, Pleiades 1/2, Quick Bird-2, Sentinel-2A/B and SPOT 6/7 have multiband sensors measuring blue, green, red and infrared bands while SPOT XS does green, red and infrared bands. LANDSAT 8 OLI has coastal (new deep blue), blue, green, red and infrared bands. WorldView-2/3/4 have coastal, blue, green, yellow, red and infrared bands. Sensors with high spectral resolution are a hyper spectral sensor. Compact airborne hyper spectral bands (CASI) have been often used for mapping coral reef ecosystems. This system is effective with a high spatial and spectral resolutions for coastal mapping. However, their cost is expensive including cost of survey with an airplane. A large quantity of data obtained by CASI requires heavy processing of data.

Table 1. Representative satellite multispectral sensors, their spatial resolutions, swath width, band spectral ranges of sensors and panchromatic bands, average revisit days and dynamic ranges. Pan and Multi are panchromatic band and multiband, respectively.

Satellite	Spatial resolution (m)	Swath width (km)	Multi and panchromatic bands (nm)		Average revisit and dynamic range
ALOS PRISM	Pan 2.5	70	NIR	760–890	46 days
AVNIR-2	Multi 10		Blue	420–500	
(from 2006 to 2011)			Green	520–600	8 bit/pixel
			Red	610–690	
			NIR	760–890	
ALOS-3 PRISM-2	Pan 0.8	70	Coastal	400–450	35 days
(launched in 2020)	Multi 3.2		Blue	450–500	
			Green	520–600	PRSIM-2
			Red	610–690	11 bit/pixel
			Red edge	690–740	
			NIR	760–890	
			Pan	520–770	
Dove (Planet)	Multi 3.7	24	Blue	455–515	Everyday
(since 2014)			Green	500–590	
			Red	590–670	12 bit/pixel
			NIR	780–860	
GeoEye-1	Pan 0.41	15.2	Blue	450–510	3 days
(since 2008)	Multi 1.64		Green	520–580	
			Red	655–690	11 bit/pixel
			NIR	780–920	
			Pan	450–900	
IKONOS	Pan 1	11.3	Blue	450–530	3 days
(from 1999 to 2015)	Multi 4		Green	520–610	
			Red	640–720	11 bit/pixel
			NIR	760–860	
			Pan	450–900	
LANDSAT ETM+	Pan 15	180	Blue	450–520	16 days
(since 1999)	Multi 30		Green	530–610	8bit/pixel
			Red	630–690	
			NIR	780–900	
			Pan	520–900	
LANDSAT 8 OLI	Pan 15	180	New Deep Blue	433–453	16 days
(since 2013)	Multi 30		Blue	450–515	
			Green	525–600	12 bit/pixel
			Red	630–680	
			NIR	845–885	
			Pan	500–860	
	Pan 0.5	20	Blue	450–530	4 days
Pleiades-1A	Multi 2.8		Green	510–590	
(since 2012)			Red	620–700	12 bit/pixel
Pleiades-1B			NIR	775–915	
(since 2013)			Pan	480–820	
QuickBird-2	Pan 0.61	16.5	Blue	450–520	3.5 days
(from 2001 to 2015)	Multi 2.4		Green	520–600	
			Red	630–690	11 bit/pixel
			NIR	760–900	
			Pan	450–900	

Table 1. Continued.

Satellite	Spatial resolution (m)	Swath width (km)	Multi and panchromatic bands (nm)		Average revisit and dynamic range
Sentinel-2A (since 2015)	Multi 10	290	Blue Green Red NIR	448–546 538–583 646–684 763–908	5 days (2A and 2B) 12 bit/pixel
Sentinel-2B (since 2017)			Blue Green Red NIR	443–541 536–582 646–685 767–900	
Spot-6 (since 2012) SPOT-7 (since 2014)	Pan 1.5 Multi 8	60	Blue Green Red NIR Pan	455–525 530–590 625–695 760–890 455–745	26 days 12 bit/pixel
WorldView-2 (since 2009) WorldView-3/4	WV-2 Pan 0.46 Mu1ti 1.85	16	Coastal Blue Green Yellow	400–450 450–510 510–580 585–625	WV-2 3.7 days 11 bit/pixel
WorldView-3/4 (since 2014/2016)	WV-3/4 Pan 0.34 Multi 1.38	13	Red Red Edge NIR1 NIR2 Pan	630–690 705–745 770–895 860–1040 450–800	WV-3 4.5 days 11 bit/pixel

3.2 Availability of satellite images and software

Non-commercial satellite images of LANDSAT TM have been archived since 1982. Downloading digital data of LANDSAT 1–5 TM, LANDSAT 7 ETM+ and LANDSAT 8 OLI can be done via internet from Landsat Data Access of United States Geological Survey (https://www.usgs.gov/land-resources/nli/landsat/landsat-data-access?qt-science_support_page_related_con=0#qt-science_support_page_related_con). Among the sites, the USGS Global Visualization Viewer (GloVis) (https://glovis.usgs.gov/) or EarthExplorer (https://earthexplorer.usgs.gov/) are easy to download LANDSAT images free of charge. Due to problem of sensor, the present LANDSAT 7 ETM+ hasn't supplied any good images for remote sensing since 2002. In 2006, non-commercial satellite, Advance Land Observation Satellite (ALOS), launched by the Japan Aerospace Exploration Agency (JAXA) has a multispectral sensor, AVNIR-2, with 10 m spatial resolution and a panchromatic sensor, PRISM, with 2.5 m spatial resolution. Image data of Sentinel-2A/B with a spatial resolution of 10 m for visible bands are also freely available via internet (https://scihub.copernicus.eu/dhus/#/home). These sensors that have spatially more precise than those of LANDSAT images permit us to map coastal areas with various ecosystems. While ALOS has been out of service since April 2011 because of electric power depletion, archives of ALOS AVNIR-2 from 2006 to 2011 are available. NASA launched LANDSAT 8 that is a successor of LANDSAT 7 in 2013. LANDSAT 8 OLI (Operational Land Imager) has higher radiometric and spectral resolutions and more visible bands, which allow us to map coastal habitats by analyzing their images. Commercial satellite images are also available. GeoEye-1, IKONOS, Planet, Pleiades-1A/B, QuickBird-2, SPOT and WorldView 2/3/4 have multiband images with very high spatial resolutions (Table 1). JAXA schedules launch of ALOS-3 in 2020.

There is a lot of commercial software for remote sensing such as ENVI, ERDAS Imagine, TNTmips, etc. Although their academic prices are reasonable, they are still expensive. Free software for remote sensing and GIS is also available via internet such as GRASS (http://grass.fbk.eu/index.php) and Multispec (https://engineering.purdue.edu/~biehl/MultiSpec/), Sentinel-2 tool box (http://step.esa.int/main/toolboxes/sentinel-2-toolbox/). QGIS (https://www.qgis.org/en/site/) is free GIS software that can be used for analyzing satellite images with a free open source plugin for QGIS. They are software to analyze satellite images as effective as commercial software.

4. Ground-truthing of Sea Bottom

Ground truth is to obtain a coverage data of location in situ corresponding to a pixel on satellite image in order to

Table 2. Satellite-based augmentation systems (SBASs) provided by a region or countries.

Country or region	Name of satellite system
Europe	European Geostationary Navigation Overlay Service (EGNOS)
USA	Wide Area Augmentation System (WAAS)
Japan	Multi-functional Satellite Augmentation System (MSAS)
India	GPS and GEO Augmented Navigation (GAGAN)
Russia	System for Differential Corrections and Monitoring (SDCM)

verify contents of the pixel on the image on land. While, in the sea, the words "sea truth" are used instead of ground truth on land, it is better to use ground truth for verifying bottom surface covers on the sea bottom. The classification of the satellite image into groups of bottom surface cover needs ground truth data as training data at supervised classification. After the classification of the image, ground truth data were used for determining an accuracy of the classification.

Ground-truthing is conducted on site, performing bottom observations and measurements of substrates covering pixels on the remotely sensed digital image. The observations require highly accurate GPS to plot substrates on the geographic coordinates. For geometric correction of image, we also measure some typical locations that we can identify on the satellite image with the highly accurate GPS. These locations are called as ground control points (GCPs) used for geometric correction. Software for remote sensing provides a function for the geometric correction with position data of GCPs as mentioned later.

Ground truth data are indispensable for a supervised classification of an image or a decision tree classification. When data of bottom cover types with location are available, they can allocate attributes of pixels corresponding to their locations on an image. The spectral characteristics of pixels of the image corresponding to bottom covers on these sites are used for decision rules for classifying the other pixels of the image. In most cases, we divide ground truth data into two groups: one for training and the other for classification success. The latter data is to make an error matrix to evaluate the accuracy of the classification.

Mapping methods of seagrass beds in situ are classified into two categories. One is a direct observation through walking, diving, grabbing, camera or video by researchers. The other is an indirect method using a remote sensing apparatus.

4.1 Determining positions of ground-truthing sites in situ

It is very important to determine geographical positions of ground-truthing sites as precise as possible because they are used for classifications and/or evaluation of classification of pixels into bottom substrate types. The Global Positioning System (GPS) became available in 1980s. It permits us to determine a geographical position of a ground-truthing site in real time. The accuracy of GPS has been ameliorated from 36 m (95% confidence level) to 6 m (95% confidence level) since 2000 because of the removal of Selective Availability (SA) from GPS (stopping the intentional degradation of the GPS signals) on 2 May 2000. In the world, 34 countries have already installed Differential GPS (D-GPS) radio beacon networks in territory of each country, and more are considering the adoption of this navigation standard. The improvement of the basic GPS signal through elimination of SA may allow the D-GPS radio beacons to transmit fewer error corrections and more accurate localization. Accuracy of D-GPS is about several decadal centimeters. However, D-GPS was abolished in Japan on 1 March 2019 because the SBAS and QZSS mentioned-below have been available (Japan Coast Guard 2017).

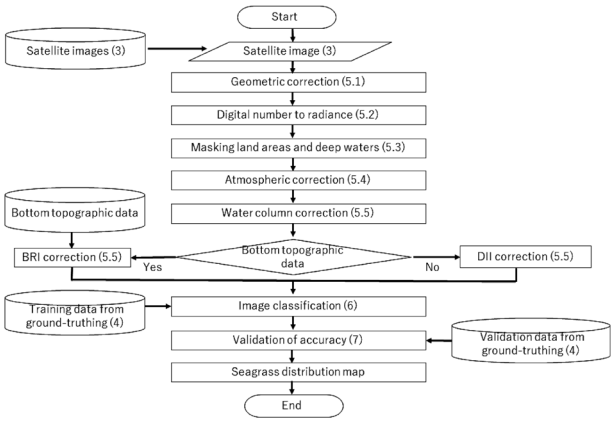

Fig. 6. Flowchart for understanding the order of each component for analyzing a satellite image and detecting seagrass distribution. Numbers in parentheses indicate chapters or sections.

Another system to ameliorate precision of positions determined with GPS is a satellite-based augmentation system (SBAS), such as European Geostationary Navigation Overlay Service (EGNOS), MTSAT Satellite-based Augmentation System of Japan (MSAS) and Wide Area Augmentation System (WAAS) of USA that are complement existing global navigation satellite systems (GNSS) (Table 2). The SBAS concept is based on GNSS measurements by accurately-located reference stations deployed across an entire continent (Fig. 6). The GNSS errors are then transferred to a comput-

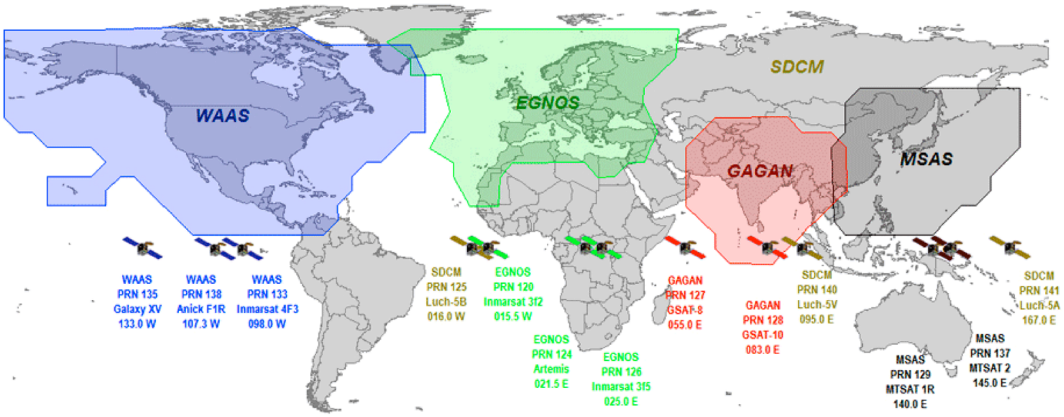

Fig. 7. Area covered by different SBAS systems in the world (source: http://sxbluegps.com/technology/sbas-made-easy/).

ing center, which calculate differential corrections and integrity messages which are then broadcasted over the continent using geostationary satellites as an augmentation or overlay of the original GNSS message. Several countries or a region have implemented their own satellite-based augmentation system as mentioned above. The SBAS can augment precision of positions within 1 m to 0.5 m.

On 11 September 2010, JAXA launched the Quasi-Zenith Satellite System (QZSS) called "Michibiki". It is a proposed three-satellite regional time transfer system and Satellite Based Augmentation System for the Global Positioning System, which can be receivable in Asia and Oceanica from 60ºE to 150ºW and from 60ºS to 60ºN including Japan. Now four Michibiki launched by JAXA fly along an orbit of eight shapes between Japan and Australia. Michibiki system runs from April 2018. It is estimated that the errors to determine positions are within 1 m. Some recent GPS can detect signals from Michibiki. Commercial products with QZSS function including GPSs, drive recorders, digital cameras etc. are listed and regularly updated at the web site of Cabinet Office of Japanese Government (https://qzss.go.jp/en/usage/products/list.html). According to this site, it is recommended to use the GPSs which can receive Michibiki, SBAS, GLObal'naya NAvigatsionnaya Sputnikovaya Sistema (GLONASS) in Russia and BeiDou Navigation Satellite System in China because more satellites give more precise positions.

4.2 Direct methods

Walking and diving

When bottom depths are less than 1 m or tidal flats emerged from the sea surface, we can walk on the bottom to observe bottom substrates with GPS. It is very easy to obtain ground truth data. On the other hand, it is needed to dive to observe the bottom when the sea level becomes high or bottom depth is deeper than 1 m. Diving belongs to direct methods and is very sure for detecting bottom substrates. A merit of diving is to identify bottom covers, especially species compositions and densities of seagrass cover. However, it is laborious and not efficient to take data at many points. It is noted that the area observed by a diver at a point is within a spatial scale of several meters. If the bottom depth is not deep, a diver can use a GPS attached to a buoy attached to the diver on the sea surface to determine its position. Calvo et al. (1993) accurately located the upper limit of *P. oceanica* meadow using a geodimeter when divers conducted ground truthing. When the bottom depth is deeper than several meters and another person measures positions of a diver from the boat with GPS, the error of positions becomes greater. This method cannot be applied to turbid water areas.

Manta tow

Manta tow is a simple method that a diver tracked by a boat takes continuous pictures as shown in Fig. 8 (e.g. Chancerelle et al. 2008, Miller et al. 2009). When a small boat is available under warm water temperature, this method is very useful to take ground truth data at places where water clarity is high. A diver towed with a boat takes pictures with a digital camera from the sea surface at intervals of several seconds. If the time of camera is synchronized with a GPS, we can map bottom pictures on a geographical chart. The GPS put in a plastic bag is fixed on the head of diver not to submerge it under the sea for receiving GPS signals.

Underwater video observation and towing

Underwater video observation is sometimes called as a drop camera observation. It is easier than diving observation. Researchers can observe bottom features with image on a display monitored with a camera lowered from a boat and recorded images to a video recorder or a computer with information through a microphone, time and date (Fig. 9). It is better that the person who lowers the camera has GPS on his pocket to identify positions of camera. Time of recorded images and GPS give position by synchronizing time of both GPS and the recorder or computer.

Towing underwater video camera system has been de-

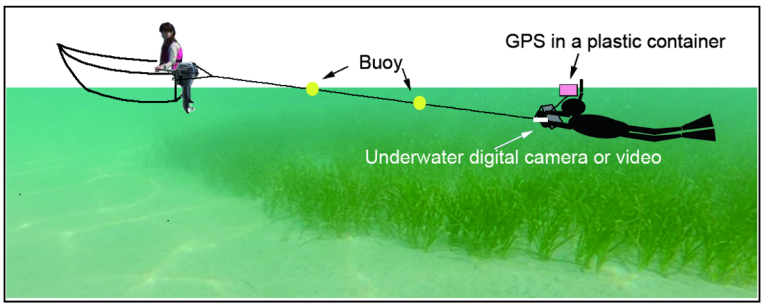

Fig. 8. A schematic view of manta tow. Yellow circles, and pink and white rectangles are buoys, GPS in a container and underwater camera or video, respectively. Buoys are attached to rope at 6 m intervals based on English et al. (1997).

Fig. 9. Photos showing video camera system for sea-truthing in Akkeshi Bay, east Hokkaido. Underwater video camera is lowered from the boat (left photo). An observer monitors bottom features by the display in the cabin (right photo).

veloped (Norris et al. 1997). The camera is mounted in a 'down-looking' orientation on a towfish, which was deployed directly off the stern of the vessel using the cargo boom. Recently, we can buy cost-effective and high-performance underwater camera such as Lumix (Panasonic Co.) and TG series (Olympus Co.) with function of interval photography and underwater video cameras such as Hero (GoPro Inc.) and Action Cam (Sony Co.). However, the method using underwater camera or video are sensitive to turbidity.

Camera or video observation from a certain altitude above the sea surface

Prof. Ken-ichi Hayashizaki, one of co-authors made ground truth surveys in Philippines. He developed a system using a digital camera or video protruding from the boat abeam, supported by a bar mounted on a bamboo pole at a height of 3 m from the boat deck (Hayashizaki and Ogawa 2011) (Fig. 10). Pictures were obtained by interval photographing. Positions of pictures were obtained with GPS by synchronizing time of camera with that of GPS. Since GoPro and Action Cam can be remotely operated with a controller through Bluetooth, it is possible to verify whether images are captured or not in real time in situ. When cameras and videos include GPS with sub-meter precision inside, it is no need to set a GPS on the top of pole or on the camera or video. Areas

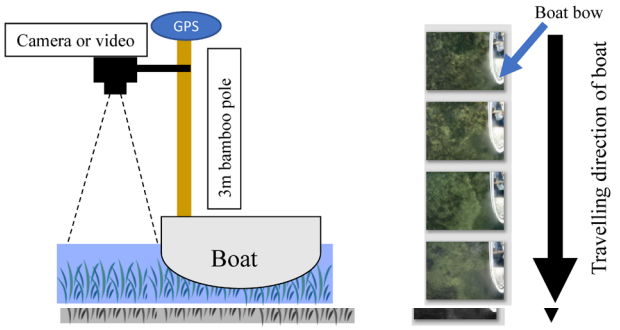

Fig. 10. Schematic diagram of a system using a digital camera or video protruding from the boat abeam, supported by a bar mounted on a bamboo pole at a height of 3 m from the boat deck (left panel) and four continual pictures obtained by the system (right panel).

of seagrass distributions can be estimated from the pictures by using a length of the boat on the pictures.

Recent advances in unoccupied aircraft systems (UAS or drones), coupled with their increased availability, present a solution of ground truth survey for satellite remote sensing. Since UAS can cover a study site with ultra-high resolution (<5 cm) imagery allowing visual validation, Gray et al. (2018) compared data of habitat distributions obtained by UAS with those obtained by ground truthing in estuarine en-

vironments. They conclude that "Considering the similarity in accuracy between UAS and field-based assessments, our conclusion is strongly in favor of validation with UAS where feasible." UAS increase sample validation points across a larger proportion of the study site, while requiring less time and less intrusion than ground truthing on the study area. Drones with a high performance are available at a reasonable price. When positions of pictures can be obtained at a submeter precision, seagrass distributions and other bottom covers are used as ground truth data. Metashape (Agisoft Co.) of which previous name was PhotoScan is a stand-alone software product performs photogrammetric processing (mosaic) of digital images and generates 3D spatial data to be used in GIS applications (https://www.agisoft.com/). This software is sold at a reasonable price.

4.3 Indirect methods

Echosounder

It is well known that acoustic backscattering information can be used to infer seafloor physical and biological properties (e.g. Hashimoto and Nishimura 1953a, Parnum and Gavrilov 2011, Tecchiato et al. 2015). However, the acoustic scatterings of seagrass and seaweed are poorly understood, compared with rock and sediment (De Falco et al. 2010). The backscattering strength of seagrass beds is usually higher than that of sandy or muddy bottoms, possibly due to gas bubbles inside the foliage, sheath and shoot stem structure (Komatsu and Tatsukawa 1998, Lyons and Abraham 1999, Sabol et al. 2002, Riegl et al. 2005, Parnum 2007, Wilson and Dunton 2009, De Falco et al. 2010, Tecchiato et al. 2015).

The echosounders have advantages not only to continuously measure biomass distributions and bottom topographies, but also to be used at a low cost and easy treatment (Komatsu et al. 2002a). This method has been applied to several studies in phanerogam beds in lakes (Duarte 1987), *Zostera marina* L. beds (Hatakeyama and Maniwa 1978, Komatsu and Tatsukawa 1998) (Fig. 11), *P. oceanica* meadows

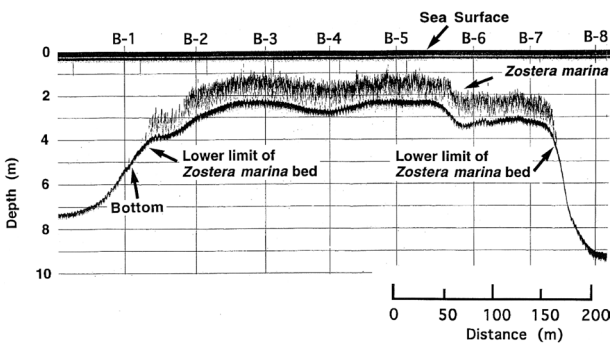

Fig. 11. Raw records of echo trace along a transact in Ajino Bay, Japan cited from Komatsu and Tatsukawa (1998). A depth of 0 m is the sea surface, which is not standardized to the depth relative to the mean sea level.

(Colantoni et al. 1982, Rey and Diaz del Rio 1989) and brown seaweed such as kelp (Hashimoto and Nishimura 1953b) and *Sargassum* species (Kitoh 1983).

Colantoni et al. (1982) tried to use a low frequency echosounder (3.5 kHz); it proved to be rather ineffective to discriminate the acoustic character between *P. oceanica* bed and the bottom. Although the high-resolution continuous seismic reflection (3.5 kHz) could distinguish the *P. oceanica* and others (Rey and Diaz del Rio 1989), long wavelength of ultrasonic brings worse vertical resolution. Echosounders with an ultrasonic wave of 200 kHz is more appropriate for detecting seagrass beds (Hatakeyama and Maniwa 1978, Komatsu and Tatsukawa 1998).

The echosounder can scan seagrass beds when traveling at about 1.0–1.5 $m\,s^{-1}$ (2–3 knots). It is possible to investigate 37 km per day when a ship with an echosounder travels at 1 $m\,s^{-1}$ (2 knots) for ten hours (Komatsu and Tatsukawa 1998). In this way, the echosounder is a very useful apparatus to map seagrass beds.

Hatakeyama and Maniwa (1978) used the echosounder for mapping a *Zostera* bed, but they calculated only an index of biomass: sum of canopy heights by unit sector along transects scanned by the echosounder. Since it is necessary to estimate seagrass or seaweed biomass for a quantitative comprehension of their ecosystems, Komatsu and Tatsukawa (1998) proposed a simple converting method from the shading grades of seagrass on echograms to above-ground biomass based on quadrat samplings (Fig. 12). From these echograms, we can extract locations of seagrass and others for satellite remote sensing.

The position of the lower bottom depth limit of seagrass beds is related to the light extinction coefficient influencing the minimum degree of light required for growth of seagrass (Duarte 1991). Thus, it can be used for an indicator of water quality. In France, the lower bottom depth limit of *P. oceanica* was monitored by placing concrete markers (Meinesz and Laurent 1978, Meinesz 1997, Boudouresque et al. 2000). In this case, obtained results are very precise, but the observed area is limited. The echosounder can be used to define the vertical distribution of seagrass bed and the lower bottom depth limit of seagrass beds by correcting depths measured by the echosounder to the sea level. Of course, it is necessary to correct sea level depending on the time based on an observatory of the tide or tide table. Monitoring seagrass by the echosounder is useful for detecting lower bottom depth limit of seagrass beds not precisely but roughly in a wide area. When these two types of monitoring are coupled, they complement each other to obtain lower bottom depth limits.

Komatsu and Tatsukawa (1998) clarified that the canopy height was nearly proportional to the maximum blade length. By cropping blades of seagrass, the height of seagrass canopies on the echo-traces can be used as an indicator of the maximum blade length of seagrass when the current speeds

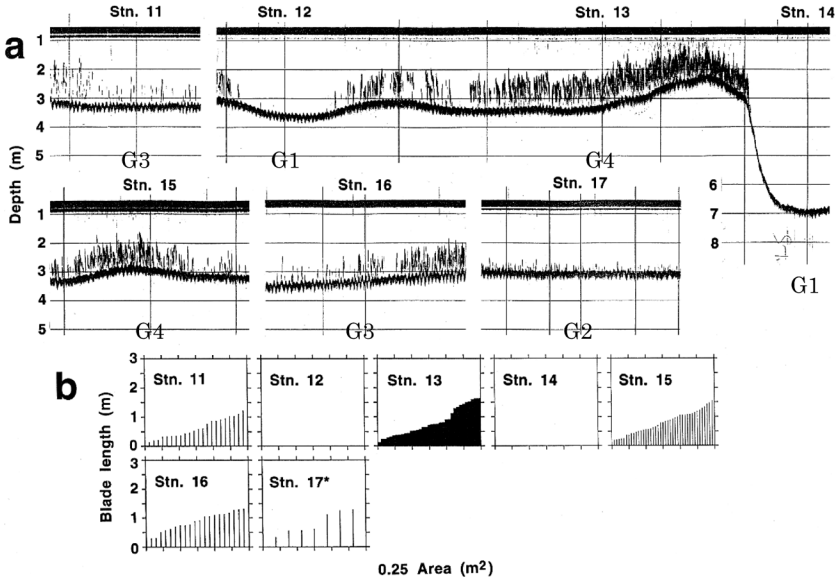

Fig. 12. Echogram (upper panels) and blade length distribution (lower panels) obtained by a quadrat sampling of 0.5 x 0.5 m at Stations 11–17 (Komatsu and Tatsukawa 1998). The mark "*" indicates transformed data from quadrat sampling of 1x1 m to that of 0.5 x 0.5 m due to small quantity of seagrass shoots. Grades of echo traces of seagrass beds were shown at the lower part of the vertical line representing the station by the following characters: G1: Grade 1 (no seagrass); G2: Grade 2 (sparse seagrass); G3: Grade 3 (intermediate dense seagrass); G4: Grade 4 (dense seagrass). Blades lengths are shown as vertical lines from the smallest one to the largest one in order in each Figure at the stations (lower panels).

were not greatly different over the beds. Tanaka and Tanaka (1985) also reported a similar proportional relation between the canopy height and maximum frond lengths of *Sargassum* species.

Sidescan Sonar

One acoustic method to map seagrass beds using a side-scan sonar, which is more efficient than that of the ground surveys, has been developed since 1970s in the Mediterranean Sea. It scanned sea bottom at a width ranging 50–500 m and could distinguish seagrass bed distributions and the others successfully (Newton and Stefanon 1975, Meinesz et al. 1981, Lefèvre et al. 1984, Gloux 1984, Ramos and Ramos-Espla 1989, Pasqualini et al. 1998). Figs. 13 and 14 show a towing apparatus of sidescan sonar and the distribution map of *Z. caulescens* in Koajiro Bay in Sagami Bay obtained by the side-scan sonar, respectively. The patch structures are clearly depicted. However, it is difficult for this method to measure heights of plants except those just beneath the transducer along a transect.

Sagawa et al. (2008) proposed use of sidescan sonar image as ground-truth data. They surveyed seagrass beds and examined accuracy of results obtained from sidescan sonar image with data obtained from drop camera observations. They verified that maps of seagrass distributions surveyed with a sidescan sonar corresponded to horizontal distributions of seagrass beds with drop camera observations and proposed to use central areas (not border areas) with and without seagrass beds as ground truthing locations because central areas of habitats with horizontal spatial scale enough broader than that of more than several satellite image pixels consist of no mixed cells of habitats above-mentioned.

Multibeam sonar

Multibeam sonar (MBS) is one of the most effective acoustic tools for mapping seagrass, because it can survey with a broad swath to create a three-dimensional (3D) image of the seagrass meadow (Komatsu et al. 2003a).

The study by Komatsu et al. (2003a) succeeded in mapping seagrass beds using bottom topography measured by a MBS for the first time. They were able to distinguish between echoes from seagrass and echoes from the actual seabed. They removed echoes from the seagrass to create a sea bottom without seagrass and subtract the sea bottom topography without seagrass from the sea bottom topography with seagrass to estimate seagrass distributions. They also estimated biomass coupling quadrat sampling of seagrass with volume and area of seagrass estimated by the MBS that flowering shoots and vegetative shoots occupied, respectively. In a different study, Komatsu et al. (2004) mapped *P. oceanica* in the Gulf of Gabes, Tunisia facing the Mediterranean Sea. They were able to differentiate the seagrass meadows of *P. oceanica* and sand beds at depths ranging from 20 to 30 m using MBS backscattering information. These studies required extensive post-processing, and multibeam sonar operation needed to be carried out by highly trained personnel due to the complexities associated with calibration and backscattering processes. In addition, the acquisition data volume

by a MBS is larger than that by echosounder and sidescan sonar processors (Anderson et al. 2008). Di Maida et al. (2011) investigated the differentiation of seagrass meadows from sandy beds using bathymetry data obtained with the MBS. They demonstrated that the MBS was capable of discriminating between *P. oceanica* meadows and sand substrate via decision-tree post-processing with use of the standard deviation of beam depths or beam depth range within the grids of the bathymetry map. The grids were classified into two categories, based on the presence or absence of high-density seagrass. Recent studies using a MBS have explored the possibility of discriminating between seagrass and macroalgae, to estimate abundance (dense or sparse) from backscattering measurements (Tecchiato et al. 2015). However, their methodology is highly complicated, and their results remain inconclusive although discrimination between the presence and absence of meadows was within acceptable limits (78% accuracy in Tecchiato et al. (2015)).

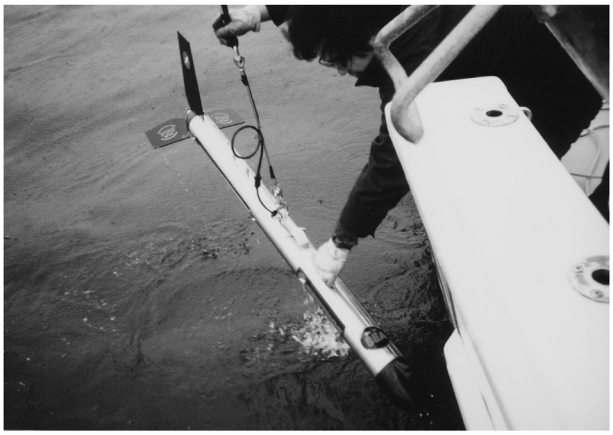

Fig. 13. Photo showing towing transducer of side-scan sonar (Komatsu et al. 2003b).

The processing and analysis of backscattering strength data from the MBS is still in the development stages. There is no standard approach for MBS application (Parnum and Gavrilov 2011). However, bathymetry data processing has advanced to the point of survey area mapping in real time (Lurton 2002). Hamana and Komatsu (2016) developed a method to map seagrass meadows and estimate their relative abundance on sand beds by using only bathymetry data which simplify post-process analysis. This system can be used to map seagrass meadows with long shoots growing in the sublittoral zone in real time with use of a hydrographical survey software with a function of 95% confidence level of bottom detections.

4.4 Seagrass cover and standing crop

Recently, satellite multiband images with high radiometric and/or spatial resolutions are obtained as explained above. Using these data, researchers have studied to create maps of seagrass cover and/or seagrass standing crop (e.g. Hashim et al. 2014). Estimation of seagrass covers or standing crop require ground truthing data. This section explains how to obtain ground-truthing data for this purpose.

Seagrass cover

In general, seagrass studies use a destructive sampling with a quadrat to examine species compositions, shoot densities, above- and below-ground biomasses, leaf lengths, leaf

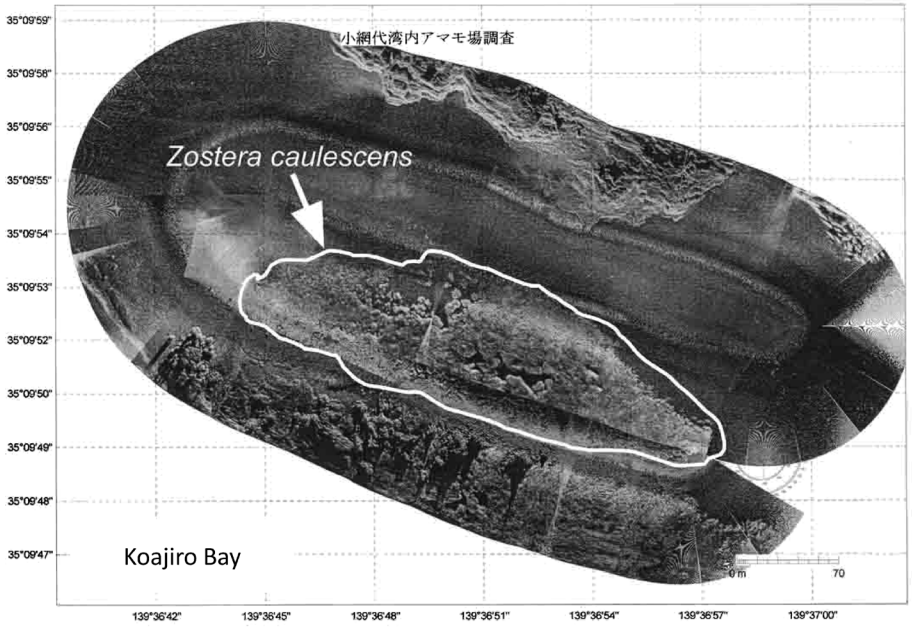

Fig. 14. Map showing horizontal distribution of *Zostera caulescens* encircled with a white line surveyed by side-scan sonar (Komatsu et al. 2003b).

area index and so on. The main disadvantage of the destructive sampling is that it takes much time to take samples in situ and analyze samples in a laboratory. Remote sensing studies require many ground truthing data. Thus, non-destructive sampling using visual assessment techniques are applied to collect data for remote sensing studies. Percentage cover of seagrass is estimated using a quadrat (e.g. McKenzie 2003). This method is to take digital pictures of seagrass on a quadrat of 0.5×0.5 m in situ and classify seagrass covers into percentage cover by using standardized pictures of seagrass covers. This method is quite repeatable when currents are weak and seagrass blades have a vertical orientation. However, the method becomes potentially unreliable when current strength increases and forces the seagrass canopy into a progressively horizontal (flattened) plane (Mumby et al. 1997a).

Seagrass standing crop

Mumby et al. (1997a) propose an alternative method to estimate seagrass standing crop based on Mellors (1991). An intensive 3-day training period was undertaken prior to a survey work. After a broad reconnaissance survey, a provisional biomass scale was established following the methods of Mellors (1991). A quadrat of 0.5×0.5 m is placed in an area with the lowest discernible biomass and was given the category 1. The next quadrat is placed in seagrass which was both densest and possessed greatest blade length. This was assigned a category of 6. Quadrats for categories 2, 3, 4 and 5 are placed by estimating a linear interpolation between categories 1 and 6. Three divers conduct surveys using the technique by haphazardly throwing quadrats and comparing categories. Over 100 quadrats are cross-compared in this fashion until inter-observer agreement is highly consistent (complete agreement on approximately 95% of occasions). At this point, an adequate 1–6 scale is deemed to have been established and 4 quadrats of each category are excavated for calibration purposes. The quadrats are located haphazardly (i.e. pseudo-randomly) and encompassed a range of seagrass species composition rates if they are more than one species.

Harvested seagrass is washed in fresh water and sorted to remove detritus and sediment. Each sample is divided by species and then sub-sampled for biomass categories 4–6 if it takes time to examine all seagrass in a quadrat of these categories. Sub-sampling is not necessary for most of the samples from categories 1–3. Epiphytes are removed from seagrass blades using either 5% citric acid or vinegar. Samples are oven-dried at 80°C for 48 h and weighed to the nearest 0.1 g using an electronic balance. Epiphyte-free total dry weights are calculated for each quadrat. It is important not to confuse percent cover or density with standing crop estimation. Although density and biomass arc closely related, the determination of standing crop also takes blade length and the relative dry weight of each species into account. From a practical perspective, the assessment is carried out by considering the entire 3-dimensional standing crop within the quadrat (i.e. a volume of seagrass above the sediment). The highest standing crop categories of 5 and 6 differ mainly in blade length rather than density. They recommend making a photographic record of the calibration quadrats which can be laminated and taken underwater for guidance.

The seagrass standing crop is plotted with ordinal scale (categories 1–6) for calibration of the scale. Mumby et al. (1997a) obtained the regression line by transforming standing crop data with a modified square root function with a good coefficient of determination. Using this regression, visual assessment surveys on seagrass can bring standing crop data.

5. Preparation for Processing Satellite Images

5.1 Geometric correction

Satellite sensors project three-dimensional surface of the earth to a plane. Satellite data were generally geocoded with WGS 84 coordinate system. Therefore, it is necessary to adjust a spherical surface to a horizontal plane. In most cases, remote sensing uses Universal Transversal Mercator (UTM) projection. In the plane of UTM, x axis and y axis represent east and north directions. UTM system has a zone number depending on longitude of an area by every six degrees from zone No. 1 between 180°W and 174°W to zone No. 60 between 174°E to 180°W. However, geometrical correction is needed to fit the image to the UTM coordinate system. This correction is based on more than six GCPs whose longitude and latitude have already been precisely obtained. In some cases, it is necessary to measure longitude and latitude of some discriminative points on the ground with a GPS with

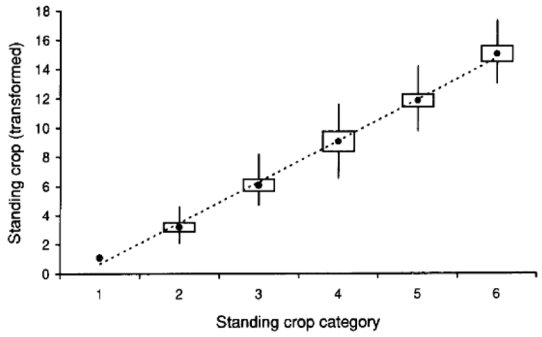

Fig. 15. Calibration of ordinal scale for estimating seagrass standing crop (Mumby et al. 1997a). The mean 95% confidence intervals of the mean and range are shown from calibration data of each category. The variance within actual dry weights has been stabilized using a modified square-root transformation ($x'=\sqrt{(x+3/8)}$). Coefficient of determination, $r^2=0.94$ (n=103), actual standing crop (g m^{-2}). (source: Mumby et al. 1997a).

precision higher than sub-meter. If no GCPs are available, we select some alternative points on the map as GSPs. We relate GCPs with the corresponding points on the satellite image with software for remote sensing. This operation is called as geometric correction. It is recommended that GCPs are scattered and also placed at edges and corners of structural object or roads for analysis.

5.2 Digital number to radiance

Raw digital number (DN) values recorded by a sensor are proportional to upwelling electromagnetic radiation. The majority of image processing has been based on DN values in which actual spectral radiances are not of interest (e.g. when classifying a single satellite image). However, there are problems with this approach. The spectral signature of a habitat expressed as DN values is not transferable because the values are image specific under viewing geometry of the satellite when the image was pictured, the location of the sun, specific weather conditions, etc. We cannot compare the values among the images taken at different time (e.g. seasons and years) by different satellite sensors and on the area of study larger than a single scene. Thus, it is necessary to convert the DN values to spectral units that are universal among different satellite images. If we obtain the spectral signature of substrate types, we can compare "spectral libraries"—i.e. libraries of spectral signatures containing lists of habitats and their reflectance. Converting the DN values to spectral units, we can refer calibration equations depending on satellite sensors that are included in the image data. In an example of IKONOS, the following conversion equation is generally used (Taylor 2005):

$$L_i = D_i / C_i, \quad (1)$$

where L is the radiance at the sensor aperture ($\mathrm{mW\,cm^{-2}\,sr^{-1}}$), C is the in-band radiance calibration coefficient ($\mathrm{cm^2\,sr\,mW^{-1}}$) and D is the DN value. In the equation the subscript i represents spectral band i. Spectral radiances can be obtained from the calibration equation (1). USGS also provides the following equation for converting DN to radiance of LANDSAT 8 OLI (USGS 2014).

$$L_i = M_{Li} D_i + A_{Li}, \quad (2)$$

where M_{Li} and A_{Li} are band-specific multiplicative rescaling factor and band-specific additive rescaling factor of band i from the metadata, respectively. These radiances are those at the top of atmosphere (TOA). DN of LANDSAT 8 OLI can be also converted to TOA reflectance as the following equation (USGS 2014):

$$\rho\lambda_i = \frac{M_{\rho i} D_i + A_{\rho i}}{\cos(\theta_{SZ})} = \frac{M_{\rho i} D_i + A_{\rho i}}{\sin(\theta_{SE})}, \quad (3)$$

where $\rho\lambda_i$ is TOA reflectance of band i. $M_{\rho i}$ and $A_{\rho i}$ are band-specific multiplicative rescaling factor and band-specific additive rescaling factor of band i from the metadata, respectively. θ_{SZ} and θ_{SE} are local sun elevation angle of the scene center in degrees provided in the metadata and local solar zenith angle, respectively.

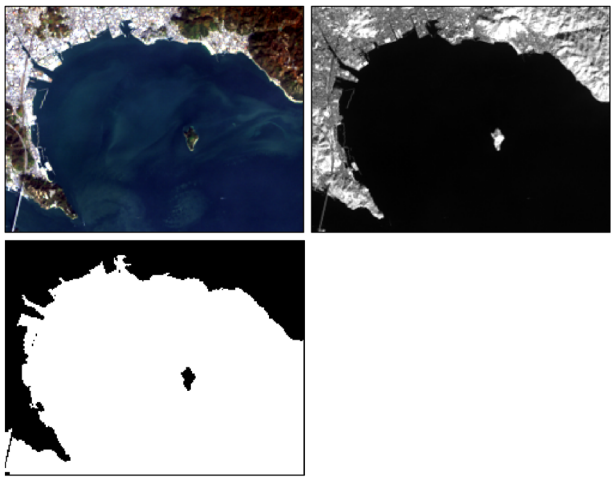

Fig. 16. LANDSAT 8 OLI images of true color (upper left), band 5 (upper right) and mask (lower) on Ajino Bay, Japan. The mask was produced from pixels with DN values of near-infra red band less than 7000.

5.3 Masking land areas and deep waters

It is necessary to exclude the land from satellite images for classification of coastal habitats to avoid miss-classification of seagrass beds. Near-infrared bands are easily absorbed by the sea surface while reflected by the land surface. Thus, we use DN, reflectance or radiance of an infrared band on the image to discriminate the sea from the land. If ponds or lakes are distributed on land, we need to manually mask them.

Deep waters are also excluded with red or green bands because they are absorbed with shallow water column. The deeper water areas indicate constantly lower values of their DN, reflectance and radiances. Thus, deep water areas can be classified with certain threshold values of red or green bands. At the same time, it is needed to pay attention not to exclude seagrass and seaweed beds because seagrass and seaweed beds also show their lower values.

5.4. Atmospheric correction

The spectral radiances are those measured at the satellite sensor. Figure 4 shows that electromagnetic radiation observed by the satellite sensor has already passed through the Earth's atmosphere twice (sun to target and target to sensor). During this passage, the radiation is affected by absorption which reduces its intensity and scattering which alters its direction. Absorption occurs when electromagnetic radiation interacts with gases such as water vapor, carbon dioxide and ozone. The electromagnetic radiation is scattered when it hits both gas molecules and airborne particulate matter (aero-

sols). Scattering will redirect incident electromagnetic radiation and deflect the reflected radiation from its path. Scattering also creates the adjacency effect in which the radiance recorded for a given pixel partly incorporates the scattered radiance from neighboring pixels. In order to make a meaningful measure of radiance at the Earth's surface, the atmospheric interferences must be removed from the data. This process is called atmospheric correction. There are some sophisticated models of atmospheric corrections such as 5s and 6s models (e.g. Tanre et al. 1990, Vermote et al. 1997), etc. After the atmospheric correction, light signals from the earth surface become clearer.

Spectral radiance will depend on the degree of illumination of the object (i.e. the irradiance). Then, the spectral radiance of features on the ground obtained by the atmospheric correction is usually converted to reflectance, which is called surface reflectance meaning the reflectance of the surface of the Earth. Be careful that the surface reflectance is not that on the sea bottom.

5.5. Water column correction

In coastal waters, Lyzenga's model has been often used for water column correction because this model's simplicity and effectiveness. In the scope of radiometric correction, each pixel value within the image (DN value) is converted into a radiance value as mentioned above. From an optical perspective, bottom type can be identified by its reflectance. According to Lyzenga (1978), the relationship between the radiance level recorded by an optical sensor and bottom reflectance is expressed by the following equation:

$$L_i = L_{si} + a_i r_i \exp(-K_i g Z), \quad (4)$$

where L is the radiance ($mW\,cm^{-2}\,sr^{-1}$) same as in the equations (1) or (2), L_s is the radiance recorded over deep water (external reflection from the water surface and scattering in the atmosphere), a is a constant which includes the solar irradiance, the transmittance of the atmosphere and the water surface, and the reduction of the radiance due to refraction at the water surface, r is the bottom surface reflectance, K is the effective attenuation coefficient of the water (m^{-1}), g is a geometric factor to account for the path length through the water and Z is the water depth (m). The subscript i means band i of image. The value of g can be geometrically calculated from the sun and satellite zenith angles at the moment when the satellite image was taken. Bottom differences are mirrored by variations in L, as r changes according to the bottom type. A radiometric correction index is required for estimating r. We introduce two types of simple radiometric correction suitable for coastal mapping: depth-invariant index proposed by Lyzenga (1981) and bottom reflectance index proposed by Sagawa et al. (2010).

Depth-invariant index

In order to remove light scattering and absorption effects within both the atmosphere and the water body, Lyzenga (1981) suggested the calculation of Depth-invariant index. This index is expressed as follows:

$$Index_{ij} = \frac{K_j \ln(L_i - L_{si}) - K_i \ln(L_i - L_{sj})}{\sqrt{K_i^2 + K_j^2}}, \quad (5)$$

where L, L_s and K are the same as in equation (4), this time with the i and j subscripts corresponding to two different bands of satellite image. Equation (5) is derived from equation (4) and refers simultaneously to two bands (bands i and j). For calculating this index, ratios of attenuation coefficients between bands are necessary. These coefficients are derived from ground truth data collected for a sandy bottom along a bottom depth gradient (Lyzenga 1981). Using ground truth data, we can plot satellite data against bottom depths for sandy bottom type. The regression curve of Lyzenga's model is then obtained. When ground truth data are not available, we estimate sandy bottom and bottom depth from the sea chart if it exists. When the sea chart is not available, we estimate K_j/K_i as follows. Equation (5) can be transformed to equation (6) through dividing numerator and denominator with K_i:

$$Index_{ij} = \frac{K_j/K_i \ln(L_i - L_{si}) - \ln(L_j - L_{sj})}{\sqrt{1 + K_j^2/K_i^2}}, \quad (6)$$

where $\ln(L_i - L_{si})$ and $\ln(L_j - L_{sj})$ are dependent variables of bottom depths from equation (4). If we can obtain reflectances of band i and j at the same pixels on a satellite image, $\ln(L_i - L_{si})$ and $\ln(L_j - L_{sj})$ on pixels interpreted as the sand bottom are plotted them on horizontal axis and vertical axis, respectively. The regression line of points between $\ln(L_i - L_{si})$ and $\ln(L_j - L_{sj})$ gives K_j/K_i as its slope. If bottom depth data are available, it is possible to bottom depth versus $\ln(L_i - L_{si})$ or $\ln(L_j - L_{sj})$. Sagawa et al. (2010) obtained very good negative exponential correlation between bottom depth and $L_i - L_{si}$ or $L_j - L_{sj}$ in Mahares, Golf of Gabes, Tunisia (Fig. 17). This shows that the regression line between $\ln(L_i - L_{si})$ and $\ln(L_j - L_{sj})$ becomes straight.

Bottom reflectance index

In order to improve mapping accuracy, Sagawa et al. (2010) proposed an alternative reflectance index (Bottom Reflectance index: BR index) expressed by the following equation:

$$BR\ index_i = \frac{(L_i - L_{si})}{\exp(-K_i g Z)}, \quad (7)$$

where L, Ls, K, g and Z are the same as equation (4).

To calculate this BR index, it is needed to combine bottom depth data, Z, with attenuation coefficient, K. We use each band attenuation coefficient same as for the Depth-in-

variant index. Concerning bottom depth data, the bathymetry map or sea chart supplied by local government or hydrographical institutions is referred. It may be reasonable to take advantage of these data, as they are easily available and represent generally accurate input. Once the numerator in equation (7) was replaced by $a_i r_i \exp(-K_i g Z)$ (from equation (4)) and the equation rearranged, the index becomes the following equation including bottom reflectance:

$$BR\ Index_i = a_i r_i \quad (8)$$

where a and r are the same as in equation (4) and i corresponds to a satellite image band i. Clearly, this index is directly related to bottom reflectance. As a result, we named it 'reflectance index'. This index enables us to compare not only the difference in reflectance ratios between bands but also the difference in absolute reflectance for each band of satellite image.

According to Lyzenga (1978), equation (4) should not be applied to very shallow areas, as the model ignores internal reflection effects occurring at the water surface. Thus, it is better to apply both radiometric corrections exclusively to areas deeper than about 1–2 m. On the other hand, we need not underwater but atmospheric radiometric correction when there are seagrasses exposed to the sea surface.

Sagawa et al. (2010) applied both radiometric corrections of Depth-invariant index and Bottom Reflectance index to IKONOS image spotting seagrass beds off Mahares in Golf of Gabes, south Tunisia, facing Mediterranean Sea, acquired on 2 October 2005. In this area, *P. oceanica* is the most abundant and common species and it mainly occurs on a sandy bottom. Figure 18 shows results of supervised classification applied to Depth-invariant index and Bottom Reflectance index to classify sand and seagrass. In these waters where attenuation coefficients of blue band and green band were 0.088^{-1} m and 0.093^{-1} m, respectively, water type was Jerlov Water Type II–III (Jerlov 1976) suggesting turbid waters (Fig. 17). Overall accuracy of the former was 54% meaning random classification between two bottom types. On the other hand, that of the latter was over 90%. When the bottom depth distribution is available, radiometric correction

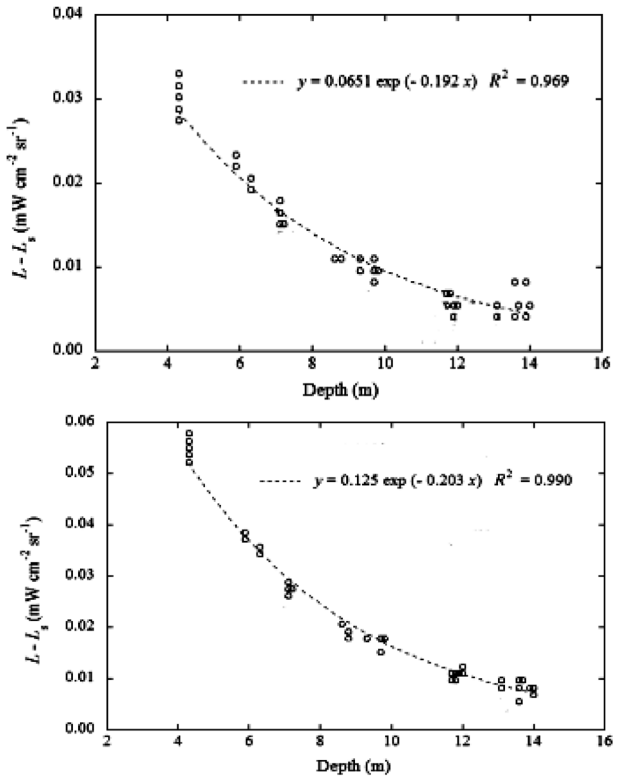

Fig. 17. Relation between bottom depths and radiance levels of blue (upper panel) and green (lower panel) on the sand bed in Mahares, Golf of Gabes, Tunisia (source: Sagawa et al. 2010).

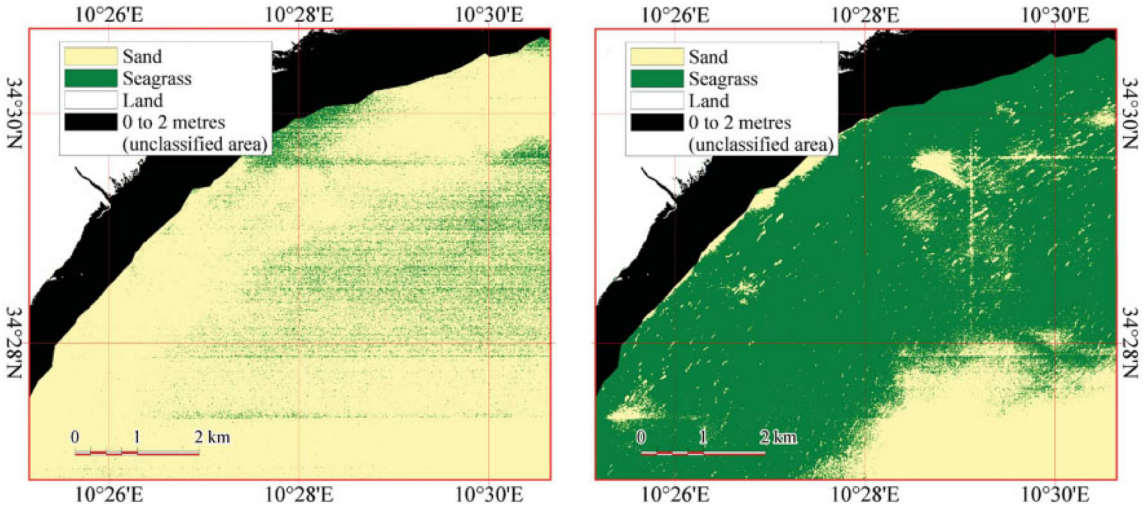

Fig. 18. Maps derived from satellite image analysis (Mahares). Black areas, described as '0–2 meters (unclassified area)' in the legends, represent the data which were not included in the analysis. The maps are obtained by applying a radiometric correction based on (a) the traditional Depth-invariant index (left map); (b) the Bottom Reflectance index (right map). (source: Sagawa et al. 2010).

using Bottom Reflectance index is very practical to map seagrass beds under turbid waters rather than Depth-invariant index. When water is clear, radiometric correction using Depth-invariant index can also obtain good classification results. This is true because some studies showed good results applying Depth-invariant index for mapping of seagrass beds in Caribbean Sea (Mumby et al. 1998) or Mediterranean Sea (Pasqualini et al. 2005, Belluco et al. 2006, Fornes et al. 2006) where transparencies are very high. Mumby and Edwards (2000) conclude that Depth-invariant index for mapping coastal habitats is applicable to only waters with high transparency belonging to Jerlov Water Type I–II (Jerlov 1976), which is roughly equivalent to waters with Secchi depth of 50 m.

6. Image Classification

6.1 Pixel-based classification

In coastal habitat mapping, pixel-based classification consisting of supervised or unsupervised classification is generally applied to multiband satellite data after radiometric correction mentioned above. Most studies on classifications for seagrass mapping have been conducted using a pixel-based analysis of satellite multiband images. They used either a supervised classification or unsupervised classification. These pixel-based procedures analyze the spectral properties of every pixel within the region of interest. Ground truth data concerning each bottom type distributions are required. These data must be prepared through ground-truthing such as diving, observation by a lowered camera from the ship, side scan sonar measurements, etc. as mentioned above and described by Komatsu et al. (2003b). If ground truth data are not available, unsupervised classification is useful. Unsupervised classification groups pixels into some categories with similar bottom reflectance through a statistical standard such as ISODATA etc. Using the unsupervised classification method, the software is instructed to create the number of clusters and the number of iterations that are inputs before processing while attempting to meet a predetermined threshold value within the number of iterations. By calculating and plotting the cluster statistics, we can determine what number of clusters (or classes) to use. Usually, we determine the number of clusters more than classes that we need. After processing, some clusters are merged to one cluster when they represent a suitable class. Based on unsupervised classification, we can effectively conduct ground truth survey or field survey.

Mumby et al. (1999) stated that the number of samples (ground truth data) necessary for one class with a supervised classification is 30 ground truth data corresponding to 30 pixels of image. Calculation of classification accuracy needs 50 ground truth data (50 pixels of image). Thus, a total of 80 ground truth data are needed for one class with a supervised classification. When we classify pixels into three classes, we need 240 ground truth data corresponding to 240 pixels of image. This is an ideal case. Since we do not have enough time to take these samples, we use 10 to 30 samples for one class for supervised classification (Green et al. 2000) and 20 to 30 samples for one class for accuracy evaluation.

The classification of supervised classification is based on the spectral signature defined in the training set. The digital image classification software determines each class on what it resembles most in the training set. Supervised classification is based on the idea that a user can select sample pixels in an image that are representative of each specific class and then direct the image processing software to use these training pixels as references for the classification of all other pixels in the image. Training pixels are based on the ground truth data above-mentioned. Supervised classification algorithms frequently used are maximum likelihood and minimum-distance classification. Maximum Likelihood method assumes that the statistics for each class in each band are normally distributed and calculates the probability that a given pixel belongs to a specific class. Each pixel is assigned to the class that has the highest probability (the maximum likelihood). Minimum Distance method uses the mean vectors for each class and calculates the Euclidean distance from each unknown pixel to the mean vector for each class. The pixels are classified to the nearest class.

Recently, machine learning and deep learning have been applied to classification of seagrass beds from satellite image. Machine Learning is a technique of parsing data, learn from that data and then apply what they have learned to make an informed decision (Anon. 2019). Deep learning is actually a subset of machine learning. The main difference between deep and machine learning is, machine learning models become better progressively but the model still needs some guidance (Anon. 2019). Machine learning uses a model such as Support Vector Machine, Random Forest, Logistic Regression etc. to acquire a relation between inputs and outputs with training data sets while deep learning uses Neural Network. If a machine learning model returns an inaccurate prediction, then the programmer needs to fix that problem explicitly, but in the case of deep learning, the model does it by himself. For example, Traganos and Reinartz (2018) applied three different methods to multispectral Sentinel-2 imagery for classifying four-class habitats (rocky algae, sand, *Cymodocea nodosa* and *P. oceanica*) in the eastern Mediterranean Sea. The machine-learning Random Forest and Support Vector Machine (SVM) methods obtained better overall accuracies than Maximum Likelihood with and without radiometric corrections. Islam et al. (2018) used deep learning methods of Convolutional Neural Network and deep Capsule Network to classify seagrass beds from 8 bands of WorldView-2 images in shallow waters in Florida State. Although

they did not apply any radiometric corrections to the images, they obtained good classification results. It seems that influence of water column on classification might be corrected through deep learning. It is necessary to increase studies on machine learning and deep learning methods to classify seagrass beds from satellite imagery by applying them to different areas.

6.2 Object-oriented classification

Recently, higher resolution satellite images such as WorldView2/3/4 are available with reasonable prices for archived images. It is possible for classifications to take the spatial or contextual information related to pixels into account. Thus, the idea to classify objects stems from pixel-based classifications to object-oriented (or object-based) classifications based on groups of pixels with based on their internal homogeneity and spectral separability at multi-scale levels. The object-oriented analysis classifies objects instead of single pixels by multi-scale segmentation of pixels, which lead to the extraction of spectrally and internally homogeneous units at a particular scale. It includes image segmentation to identify image objects and classification of the identified image objects. Objects form a hierarchical and scale-dependent structure. This means that any object, in contrast to a pixel, has not only neighbors but also sub-objects and super-objects at different scales. Groups of pixels, due to their hierarchical structure, are able to include many attributes which can describe objects' intrinsic characteristics (using physical features like color, texture, and shape), typological characteristics (relations to other objects, sub-objects and super-objects) and context. Representative softwares of object-oriented approach are ArcGIS 10 (Esri), ENVI EX (Exelis VIS) and eCognition (Trimble), which are based on edge to identify image objects and on FNEA (fractal net evolution approach) and multi-resolution segmentation, respectively (Xiaohe et al. 2014).

The object-oriented method was applied to seagrass mapping with images obtained from airborne digital cameras by Lathrop et al. (2006). Following Robbins and Bell (1994) approach, they set habitat structure at three different levels: (a) meadow - a spatially continuous area of seagrass beds of varying percent of cover composition; (b) bed—a spatially continuous area of overall similar percent of cover composition; and (c) patch—a small discrete clump of seagrass- or gap—an area within a seagrass bed not occupied by plants.

Lathrop et al. (2006) developed a hierarchical classification scheme to multiband images in a shallow (mean depth of 1.5 m at mean lower-low water) back-bay lagoonal type of estuary on New Jersey's Atlantic coast taken by an airborne digital camera. Two GeoTiff image products were created: a true color imagery set, and an infrared imagery set, both at a 1-meter ground cell resolution and 8-bit radiometric resolution. They broadened three different levels of seagrass to six levels: Level 1 of land and water, Level 2 of deep water/channels (>1.5 to 2 m depth) and shallow water (<1.5 to 2 m depth) from water of Level 1, Level 3 of sand/mud flats (<1.5 to 2 m depth) and macrophyte from shallow water of Level 2, Level 4 of the macroalgae and seagrass meadows from macrophyte of Level 4, Level 5 of dense, moderate and sparse seagrass beds from seagrass meadows of Level 4, and Level 6 of seagrass patch and gap (bare bottom) of three seagrass levels of Level 5. Level 1 was classified with near-infrared band. Level 2 was classified a simple membership rule based on the bathymetry layer. Level 6 was obtained by segmenting the whole area to fine scale objects using a scale parameter of 10. The image segmentation was then coarsened to merge areas of like classes using a scale parameter of 15 (for Level 5) and 30 (for Level 4). The Level 4 or 5 image objects were visually interpreted, and manual encoded as to the appropriate bottom type based on the analyst judgment. If the field reference data was available, the analyst can consult them. Thus, level 4 to 6 are dependent of scales of image segmentation decided by scale parameters arbitrarily given. The size of the object is associated with its physical and biological spatial structure. A homogeneity criterion for smoothness and compactness of segmentation is based on a local variance of pixels to be grouped, given by a parameter. The seagrass density data for the 245 field reference points were categorized into four seagrass density classes (absent, sparse, moderate and dense), compared with the same location from the classification result.

Urbański et al. (2010) analyzed Quickbird data for mapping seagrass beds in sandy shoal habitat in the southern Baltic Sea. The spatial resolution of the panchromatic band and multi-spectral bands are 0.6 m and 2.5 m, respectively. Their number and size at the particular segmentation level depend on a scale parameter. The segmentation process aims to retain objects of strong spectral and shape homogeneity. They segmented each panchromatic image for the following scale parameters: 400, 300, 200, 100, 50, and 20, which constitute six levels of objects as mentioned above. The homogeneity criterion was set to 0.9 for colour, 0.1 for shape, and 0.5 both for smoothness and compactness. They selected level of seagrass meadows, beds and patch/gap with scale parameters of 200, 20 and 10, respectively. They classified segments of seagrass bed level into five zones with a seagrass index (SGI) consisting of band 1, band 2 and standard deviation of band 2 of segment with a scale parameter of 20. Within each zone in the object layer with a scale parameter of 20 (patch/gap level), approximately 30 objects presenting vegetation cover (Submerged Aquatic Vegetation: SAV) and approx. 30 objects without vegetation cover (not SAV) were selected by manual sampling. In order to perform accuracy assessments, samples from the patch/gap level were selected once more but for the scale parameter of 10. The samples were assigned to SAV or not SAV classes. They stated "Atypical, poten-

tially difficult to classify objects were purposely chosen". A problem of object-oriented classification is to set parameters not objectively but subjectively and also needs manual choosing of segments. In many cases, seagrasses grow patchily. Thus, it isn't problem that seagrass maps obtained by a pixel-based classification applying satellite images with a high spatial resolution show their distributions as salt-and-pepper.

7. Validation of Accuracy

One of the most important themes for seagrass mapping with remote sensing is an accuracy evaluation of classification. In general, accuracies of classification are evaluated with an error matrix (confusion matrix or contingency table) (Mumby and Green 2000). The accuracies are judged with a user accuracy, a producer accuracy, an overall accuracy and a tau coefficient (Ma and Redmond 1995).

7.1 Error Matrix (Pixels and percent)

The error is calculated by comparing the class of each ground truth pixel with the corresponding class in the classification image. Each column of the error matrix represents a ground truth class and the values in the column correspond to the classification image's labeling of the ground truth pixels. Table 3 shows the class distribution in pixels and percentage for each ground truth class.

The user accuracy is a measure indicating the probability that a pixel is Class A given that the classifier has labeled the image pixel into Class A. User accuracies are shown in the rows of the error matrix. For example, in Table 3, seagrass pixels obtained with a ground survey are 50 of which 39 and 11 are correctly and incorrectly classified, respectively. The percentages of the number of pixels correctly and incorrectly classified into the seagrass class were 78% and 22% (Table 3), respectively, corresponding to a user accuracy and an error of commission.

The producer accuracy is a measure indicating the probability that the classifier has labeled an image pixel into Class A given that the ground truth is Class A. For example, in Table 3, seagrass class of ground truth has a total of 48 pixels of which 39 and 9 pixels are correctly and incorrectly classified, respectively. The percentages of the number of seagrass pixels obtained with the ground survey classified correctly and incorrectly are 81.3% and 18.8%, respectively, corresponding to a producer accuracy and an error of omission (Table 1).

The overall accuracy is calculated by summing the number of pixels classified correctly and dividing by the total number of pixels. The pixels correctly classified are found along the diagonal of the error matrix table which lists the number of pixels that were classified into the correct ground truth classes. The total number of pixels is the sum of all the pixels in all the ground truth classes. For example, in Table 3, the pixel counts of diagonal components consist of 39 pixels of seagrass and 51 pixels of sand, which are correctly classified pixels. The overall accuracy (81.8%) is obtained by dividing the correctly classified pixels number (39+51) by the total number of ground truth pixels (110).

The overall accuracy is the overall degree of agreement in the matrix. Generally, accuracies of classification of surface covers of coastal sea bottom are lower than those of land (e.g. Mumby et al. 1998). Mumby et al. (1999) stated that a reasonable accuracy is between 60 and 80% for coarse descriptive resolution such as corals/seagrasses and mangroves/non-mangroves by using satellite images such as LANDSAT TM or pansharpened image of LANDSAT TM with SPOT. In any cases, overall accuracy is more than about 90% to monitor temporal changes in spatial distributions of bottom covers using a remote sensing (Mumby and Green 2000).

7.2 Tau coefficient

It is a reasonable way to describe the overall accuracy of a map but does not account for the component of accuracy resulting from chance alone. A chance component of accuracy exists because even a random assignment of pixels to habitat classes would include some correct assignments.

The Tau coefficient, $T(e)$, is another measure of the accuracy of the classification to exclude a chance component and is expressed as the following equation:

Table 3. Example of error matrix of seagrass mapping. Shaded cells represent diagonal components that are correctly classified. Numbers and those in parentheses are pixels and percentages of pixels, respectively.

Satellite image classification data	Ground truth			
	Seagrass	Sand	Row total	User accuracy
Seagrass	39 (35.5)	11 (10)	50 (45.5)	39/50 (78)
Sand	9 (8.2)	51 (46.3)	60 (54.5)	51/60 (85)
Column total	48	62	110 (100)	
Producer accuracy	39/48 (81.2)	51/62 (82.3)		
Overall accuracy			90/110 (81.8)	
Tau coefficient			0.636	

$$T(\mathrm{e}) = \frac{Pr(\mathrm{a}) - Pr(\mathrm{e})}{1 - Pr(\mathrm{e})}, \quad (9)$$

where Pr(a) and Pr(e) are the relative observed agreement among classes and hypothetical probability of chance agreement, respectively. For example, in Table 3, Pr(a) corresponds to the overall accuracy, 0.818. Pr(e) derived from two classes is 0.5. Then, we can obtain T(e) as 0.636 by dividing (0.818–0.50) with (1.0–0.5). The Tau coefficient ranges between −1.0 and 1.0. When the Tau coefficient is −1.0 and 1.0, classification is of perfect discrepancy and agreement, respectively. When the Tau coefficient is between 0.41 and 0.60, classification is of moderate agreement. When the Tau coefficient is between 0.61 and 0.80, classification is of good agreement. When the Tau coefficient is over 0.80, classification is of nearly prefect agreement.

The variance of Tau, σ^2, is calculated as the following equation (Ma and Redmond 1995):

$$\sigma^2 = \frac{Pr(\mathrm{a})\,(1 - Pr(\mathrm{a}))}{n(1 - Pr(\mathrm{e}))^2}, \quad (10)$$

where n is the number of samples. Confidence interval (CI) is then calculated for each Tau coefficient at the 95% confidence level ($1-\alpha$), using the following form:

$$95\%\mathrm{CI} = T(e) \pm Z_{\alpha/2}(\sigma^2)^{0.5}, \quad (11)$$

where Z is a standard normal distribution with the lower bound of $\alpha/2$. Using Table 3, we obtain 95%CI as 0.636 ±0.001. The coefficient's distribution approximates to normality and Z-tests can be performed to examine differences between matrices (Ma and Redmond 1995). When two different classification methods (method 1 and method 2) are applied, Z-tests are conducted to verify whether significant difference in Tau coefficients (T_1 and T_2) between results obtained by method 1 and method 2 exists or not using the following equations:

$$Z = \frac{T_1 - T_2}{\sqrt{\sigma_1^2 - \sigma_2^2}}, \quad (12)$$

where σ^2 is the variance of the Tau coefficient, calculated from equation (10). We can examine whether Tau coefficients have a 95% probability of being different or not.

8. Coverage and Biomass Estimation of Seagrass

Some recent studies have documented methods for mapping seagrass species, cover and biomass properties from satellite images and field data (e.g. Urbański et al. 2010, Baumstark et al. 2013). Phinn et al. (2008) compared accuracies of seagrass percentage cover classification (1–10%, 10–40%, 40–70% and 70–100%) in the shallow subtidal areas of the Eastern Banks, Moreton Bay, Australia, among images of compact airborne spectrographic imager with a pixel size of 4 m×4 m, a radiometric resolution of 14 bit and 16 bands (CASI), QuickBird-2 with a pixel size of 2.4 m×2.4 m, a radiometric resolution of 11 bit and 4 bands, and LANDSAT 5 TM with a pixel size of 30 m × 30 m, a radiometric resolution of 8 bit and 4 bands. The airborne hyper-spectral image data returned high accuracies across all cover levels from very high (70–100%) to very sparse (0–10%). In contrast, both QuickBird-2 and LANDSAT 5 TM were unable to differentiate moderate to low (10–40%) and sparse (0–10%) levels of seagrass cover. In the LANDSAT 5 TM image data, this was caused by a function of its relatively large pixel size, limited radiometric resolution and broad spectral bands. Phinn et al. (2008) stated that the band placement and slightly lower radiometric resolution of QuickBird-2 than the CASI data reduced its ability to detect the small reflectance differences between seagrass cover.

Most of researches on seagrass biomass use relation between signals of multibands from bottom substrates and seagrass covers or standing crops of seagrass. Seagrass covers and standing crops of seagrass are obtained by quadrat sampling of seagrass through field surveys. Mumby et al. (1997b) used the Depth-invariant index (DII) as signals. They applied principal component analyses to combine multiple DIIs into a single regressor (the first principal component). They obtained ground-truthing data by simple, precise, non-destructive and quick method for measuring seagrass standing explained in Section 4.4.

Above-ground biomass of seagrass has been estimated by remote sensing. Most of studies have converted pixel values of reflectance to above-ground biomass based on a regression between reflectance and biomass which have been obtained by quadrat sampling in situ. Mumby et al. (1997b) compared performances of above-ground biomass estimation with use of regressions between field measurements of standing crop and DIIs of LANDSAT TM, SPOT XS and CASI images on seagrasses in the tropical Western Atlantic. They found that predictions were high coefficients of determination: 0.74, 0.79 and 0.81, respectively.

Hashim et al. (2014) used LANDSAT 8 OLI image to map seagrass biomass in Johor Straight. After they classified seagrass beds, they mapped above-ground biomass of classified seagrass area based on a regression between BR Index and above-ground biomass of quadrat sampling of 0.5 × 0.5 m. They obtained good regression between them with a coefficient of determination of 0.93 (r^2) (see Fig. 13).

For estimating above-ground biomass of seagrasses, it is necessary to consider their seasonal changes. When we compare biomass distributions among different locations and periods, we need to take luxurious and scanty growth seasons of seagrasses, interannual changes of timing of their growth and interannual changes in their distributions into account.

Another problem is whether quadrat sampling of seagrass biomass in only 0.5×0.5 m area represents biomass in a pixel or not. For example, one pixel of LANDSAT TM is 30 × 30 m. This pixel size includes not only quadrat sampling position but also other bottom covers, which produce a mixed pixel. If seagrass beds are not homogeneous, quadrat samples are not representative of the pixel because of its broader area. If we use QuickBird-2 or CASI, we encounter georeferencing problems of quadrat samples in situ and pixels of an image. In general, positions of quadrat sampling are determined with GPS including an error. Satellite and CASI images also include error in pixel positions. It is possible that a position of quadrat sampling is not identical to a pixel on satellite or CASI images. To solve this georeferencing problem, it is needed to use more accurate GPS system having a QZSS system and also to conduct a quadrat sampling of a macrophyte at places where seagrass is homogeneously and broadly distributed. In this case, image obtained by a side-scan sonar can be used to evaluate a growth condition indicated by Sagawa et al. (2008).

9. Summary

Most of remote sensing studies on seagrass beds aim to map not only spatial distributions at a certain time but also temporal changes in spatial distributions from time to time. To conduct a reliable assessment of changes in seagrass extent and cover over time, the data sets compared should be based on specific requirements as shown in Table 4 (Roelfsema et al. 2013). For assessing natural variability of seagrass distribution (intra- and inter-annual variations), it is important that field sampling data and location, and date of remotely sensed data sets are considered.

We introduced simple and practical methods to map seagrass beds with satellite remote sensing. It is stressed that radiometric correction is very important for satellite remote sensing to correctly map bottom types. In tropical waters, water transparency is usually very high. A simple method of Lyzenga's DII is very useful. On the other hand, in temperate waters with low transparency, the Bottom Reflectance index (BRI) method proposed by Sagawa et al. (2010) is better than the DII method to map seagrass beds by satellite remote sensing when bottom topography data are available.

At this moment, LANDSAT 8 OLI and Sentinel-2 with 30 m and 10 m spatial resolution are the only freely available non-commercial satellite images provided by NASA and ESA, respectively and can be applied to coastal habitat mapping without cost. In fiscal 2020, JAXA will launch ALOS-3 that has higher spatial resolution of 4 × 4 m than LANDSAT 8 OLI and Sentinel-2. When this satellite is successfully launched in 2020, seagrass mapping in not only Asia and the Northwest Pacific but also the other regions will be advanced enormously under the condition that Japanese Government provides such images in free to everybody for contributing Sustainable Development Goal 14.

Acknowledgements

This review was based on the results from several workshops of Ocean Remote Sensing Project of Coastal Habitat Mapping (ORSP-CHM) since 2010 under the IOC Sub-Commission for the Western Pacific (WESTPAC), the Intergovernmental Oceanographic Commission of the United Nations Educational, Scientific and Cul-

Table 4. Ideal requirements to conduct a reliable assessment of changes in seagrass extent and horizontal projected percentage seagrass cover over time. *The error that could occur when requirement is not adhered to (Source: Roelfsema et al. 2013).

Data set requirement	Error type	Example of impact error (DS1=data set 1, DS2=Data set 2)
Georeferenced	Position shift	Detected changes (false positive)
Near identical spatial extent	Missing data	If an area is not mapped for DS1 compared to DS2 due to missing data, it could be detected as a change
Identical mapping categories	Incomparable mapping categories	Qualitative versus quantitative categories
Identical mapping scale	Variation in level of detail	Small patches of seagrass are mapped in one and not in other
Reproducible mapping method	Methodological error	DS1 based on manual digitization, DS2 based on pixel-based image classification
Seasonal sampling	Natural variation	DS1 in winter and DS2 in summer
Similar tidal stage and water clarity	Affects ability to detect seagrass	Satellite image for DS1 was derived at high tide with turbid water, and for DS2 with low tide and clear water. Seagrass could be mapped in deeper water for DS2.
Replicate field sampling	Variation in calibration or validation	DS1 field data based on limited point-based sampling, DS2 based on detailed transect sampling for same area
Sampling accuracy	Decreased map quality	DS1 has high accuracy versus DS2 with low accuracy resulting in low reliability

tural Organization (IOC/UNESCO). The original manuscript was presented for the workshop on case studies on seagrass mapping in the selected sea areas in the NOWPAP region organized by the Action Plan for the Protection, Management and Development of the Marine and Coastal Environment of the Northwest Pacific Region (NOWPAP) as a part of the Regional Seas Programme of the United Nations Environment Programme (UNEP) in August 2015. The authors thank to Ministry of Education, Sports, Culture and Science of Japan for providing Japan Fund in Trust for "Promoting the Awareness on Coastal Marine Environmental Changes and its Impact (2011–2013)", "Bolstering Knowledge and Institutional Capacity for Ensuring Marine Biodiversity and Seafood Security (2014–2017)" and "Accelerating the transfer of marine technology for the conservation and sustainable use of oceans, seas and marine resources (2018–2021)" to organize the workshops. These workshops were also supported by Japan Society for the Promotion of Science-Asian Core Program on Establishment of Research and Education Network on Coastal Marine Science in. Southeast Asia (JSPS-COMSEA) led by Prof. Shuhei Nishida of the University of Tokyo. The authors appreciate Prof. Tom Morris of Fullerton College, California, USA who kindly provided Figure 3 to this article. Finally, they acknowledge to Mr. Wenxi Zhu, Head of IOC/WESTPAC Office, Prof. Emeritus Yasuwo Fukuyo of the University of Tokyo, former Vice Chairperson of WESTPAC and Prof. Emeritus Tetsuo Yanagi of Kyushu University, former leader of JSPS project for their support to have the workshops and their encouragements to conduct the ORSP-CHM since 2010.

References

Anderson, J. T., van Holliday, D., Kloser, R., Reid, D. G. and Simard, Y. 2008. Acoustic seabed classification: Current practice and future directions. ICES J. Mar. Sci. J. Cons. 65: 1004–1011.

Anon. 2019. Artificial intelligence vs Machine Learning vs Deep Learning. https://www.geeksforgeeks.org/artificial-intelligence-vs-machine-learning-vs-deep-learning/ accessed on 1 May 2019.

Baumstark, R., Dixon, B., Carlson, P., Palandro, D. and Kolasa, K. 2013. Alternative spatially enhanced integrative techniques for mapping seagrass in Florida's marine ecosystem. Int. J. Remote Sens. 34: 1248–1264.

Belluco, E., Camuffo, M., Ferrari, S., Modenese, L., Silvestri, S., Marani, A. and Marani, M. 2006. Mapping salt-marsh vegetation by multispectral and hyperspectral remote sensing. Remote Sens. Environ. 105: 54–67.

Boudouresque, C.-F., Charbonel, E., Meinesz, A., Pergent, G., Pergent-Martini, C., Cadiou, G., Bertrandy, M. C., Foret, P., Ragazzi, M. and Rico-Raimondino, V. 2000. A monitoring network based on the seagrass *Posidonia oceanica* in the northwestern Mediterranean Sea. Biol. Mar. Mediterr. 7: 328–31.

Calvo, S., Frada Osterano, C. and Abbadessa, P. 1993. The suitability of a topographical instrument for an integrated approach to the cartography of *Posidonia oceanica* meadows. Oceanol. Acta 16: 273–278.

Chancerelle, Y., Maurin, R., Poujade, S. and Vieux, C. 2008. Photo tow: a new method for estimating coral reef status and changes at large spatial scale. A coral bleaching event case study. J. Soc. Océanis., 126–127. http://journals.openedition.org/jso/3312; DOI:10.4000/jso.3312

Colantoni, P., Gallignani, P., Fresi, E. and Cinelli, F. 1982. Patterns of *Posidonia oceanica* (L.) Delile beds around the Island of Ischia (Gulf of Naples) and in adjacent waters. P.S.Z.N.: Mar. Ecol. 3: 53–74.

Coles, R. G., Lee Long, W. J., Watson, R. A. and Derbyshire, K. J. 1993. Distribution of seagrasses, and their fish and penaeid prawn communities, in Cairns Harbour, a tropical estuary, northern Queensland, Australia. Austral. J. Mar. Fresh. Res. 44: 193–210.

Costanza, R., d'Arge, R., de Groot, R., Farber, S., Grasso, M., Hannon, B., Limburg, K., Naeem, S., O'Neill, R. V., Paruelo, J., Raskin, R. G., Sutton, P. and van den Belt, M. 1997. The value of the world's ecosystem services and natural capital. Nature 387: 253–260.

De Falco, G., Tonielli, R., di Martino, G., Innangi, S., Simeone, S. and Parnum, I. M. 2010. Relationships between multibeam backscatter, sediment grain size and *Posidonia oceanica* seagrass distribution. Cont. Shelf Res. 30: 1941–1950.

Dennison, W. C., Orth, R. J., Moore, K. A., Stevenson, J. C., Carter, V., Kollar, S, Bergstrom, P. W. and Batiuk, R. A. 1993. Assessing water quality with submerged aquatic vegetation: Habitat requirements as barometers of Chesapeake Bay health. BioSci. 43: 86–94.

Di Maida, G., Tomasello, A., Luzzu, F., Scannavino, A., Pirrotta, M., Orestano, C. and Calvo, S. 2011. Discriminating between *Posidonia oceanica* meadows and sand substratum using multibeam sonar. ICES J. Mar. Sci. 68: 12–19.

Dierberg, F. E. and Kiattisimkul, W. 1996. Issues, impacts, and implications of shrimp aquaculture in Thailand. Environ. Manage. 20: 649–666.

Duarte, C. M. 1987. Use of echosounder tracings to estimate the above ground biomass of submerged plant in lakes. Canad. J. Fisher. Aquat. Sci. 44: 732–735.

Duarte, C. M. 1991. Seagrass depth limits. Aquat. Bot. 40: 363–377.

English, S., Wilkinson, C. and Baker, V. (eds.) 1997. Survey manual for tropical marine resources, 2nd edition. Australian Institute of Marine Sciences, Townsville, Australia.

Fredj, G., Meinardi, M., Pierrot, S. and Roy, P. 1990. Cartographie par le satellite SPOT 1 de communautés benthiques littorales en Méditerranée occidentale. Bull. Inst. Oceanogr. Monaco 6: 71–85.

Fornes, A., Basterretxea, G., Orfila, A., Jordi, A., Alvarez, A. and Tintore, J. 2006. Mapping *Posidonia oceanica* from IKONOS. ISPRS J. Photogram. Remote Sens. 60: 315–322.

Gloux, B. 1984. Méthode acoustiques et informatiques appliquées à la cartographie rapide et détaillée des herbiers. *In* International Workshop on *Posidonia oceanica* beds. Boudouresque, C.-F., Jeudy de Grissac, A. and Olivier, J. (eds.), pp. 45–48, GIS Posidonie Press, Marseille.

Gray, P. C., Ridge, J. T., Poulin, S. K., Seymour, A. C., Schwantes, A. M., Swenson, J. J. and Johnston, D. W. 2018. Integrating drone imagery into high resolution satellite remote sensing assessments of estuarine environments. Remote Sens. 10(8): 1257. https://www.mdpi.com/2072-4292/10/8/1257/pdf

Green, E., Clark, C. and Edwards, A. 2000. Image classification and habitat mapping. *In* Remote sensing handbook for tropical coastal management. Edwards, A. J. (ed.), pp. 155–174,

UNESCO, Paris.

Gujja, B. and Finger-Stich, A. 1996. What price prawn? Shrimp aquaculture's impact in Asia. Environ. 38: 12–39.

Haddad, K. D. and Harris, B. A. 1985. Use of remote sensing to access estuarine habitats. *In* Proceeding of the Fourth Symposium on Coastal and Ocean management "Coastal Zone '85", pp. 662–675, ASCE, Baltimore, July 30-August 1. https://repository.library.noaa.gov/view/noaa/9221/noaa_9221_DS1.pdf

Hamana, M. and Komatsu, T. 2016. Real-time classification of seagrass meadows on flat bottom with bathymetric data measured by a narrow multibeam sonar system. Remote Sens. 8: 96. doi: 10.3390/rs8020096

Hashim, M., Misbari, S., Yahya, N. N., Ahmad, S., Reba, M. N. and Komatsu, T. 2014. An approach for quantification of submerged seagrass biomass in shallow turbid coastal waters. *In* Geoscience and Remote Sensing Symposium (IGARSS), pp. 4439–4442, 2014 IEEE International, IEEE.

Hashimoto, T. and Nishimura, M. 1953a. Sounding of artificial schools, rocks and sea plants fields by fish finder. Tech. Rep. Fishing Boat Lab. 4: 138–142. (in Japanese).

Hashimoto, T. and Nishimura, M. 1953b. Study on detection of Japanese tang field by the ultrasonic fish-finder. Tech. Rep. Fishing Boat Lab. 5: 187–194. (in Japanese).

Hatakeyama, Y. and Maniwa, Y. 1978. On the investigation of seaweed distribution by utilizing the fish finder. Tech. Rep. Fishing Boat Lab. 73: 155–168. (in Japanese).

Hayashizaki, K. and Ogawa, H. 2011. Underwater observation on seagrass communities. *In* Seagrasses: Resource status and trends in Indonesia, Japan, Malaysia, Thailand and Vietnam. Ogawa, H., Japar Sidik, B. and Muta Harar, Z. (eds.), pp. 132–152, Seizsando-Shoten, Tokyo.

Huitric, M., Folke, C. and Kautsky, N. 2002. Development and government policies of the shrimp farming industry in Thailand in relation to mangrove ecosystems. Ecol. Econo. 40: 441–455.

Islam, K. A., Pérez, D., Hill, V., Schaeffer, B., Zimmerman, R. and Li, J. 2018. Seagrass detection in coastal water through deep capsule networks. *In* Chinese Conference on Pattern Recognition and Computer Vision (PRCV), pp. 320–331, Springer, Cham.

Japan Coast Guard. 2017. About the abolition of differential GPS. Japan Coast Guard, Tokyo. (in Japanese). https://www.kaiho.mlit.go.jp/soshiki/koutsuu/dgps/haishi.pdf

Jerlov, N. G. 1976. Marine Optics. Elsevier Scientific Pub., New York.

Jeudy de Grissac, A. and Boudouresque, C.-F. 1985. Rôle des herbiers de Phanérogames marines dans les mouvements des sédiments côtiers: les herbiers à *Posidonia oceanica*. *In* Acte du colloque pluridisciplinaire franco-japonais d'Océanographie Fiscicule 1. Ceccaldi, H. J. and Champalbert, G. (eds.), pp. 143–151, Société Franco-japonaise d'Océanographie, Marseille.

Kirkman, H. 1996. Baseline and monitoring methods for seagrass meadows. J. Environ. Manag. 47(2): 191–201.

Kitoh, H. 1983. Seaweed beds research by a scientific echosounder. Seikai Regional Fish. Res. Inst. News 43: 2–4. (in Japanese).

Komatsu, T. 1989. Day-night reversion in the horizontal distributions of dissolved oxygen content and pH in a *Sargassum* forest. J. Oceanogr. Soc. Jpn. 45: 106–115.

Komatsu, T. 1996. Influence of a *Zostera* bed on the spatial distribution of water flow over a broad geographical area, *In* Seagrass biology: Proceedings of an international workshop Rottnest Island, Western Australia, 25–29 January 1996. Kuo, J, Phillips, RC, Walker DI. and Kirkman, H. (eds.), pp. 111–116, Faculty of Science, The University of Western Australia, Nedlands.

Komatsu, T. 1997. Long-term changes in the *Zostera* bed area in the Seto Inland Sea (Japan), especially along the coast of the Okayama Prefecture. Oceanol. Acta 20: 209–216.

Komatsu, T. and Tatsukawa, T. 1998. Mapping of *Zostera marina* L. beds in Ajino Bay, Seto Inland Sea, Japan, by using echo-sounder and global positioning systems. J. Recherche Océanogr. 23: 39–46.

Komatsu, T. and Yamano, H. 2000. Influence of seagrass vegetation on bottom topography and sediment distribution on a small spatial scale in the Dravuni Island Lagoon, Fiji. Biol. Mar. Mediter. 7: 243–246.

Komatsu, T., Ben Mustapha, K., Shibata, K., Hantani, K., Ohmura, T., Sammari, C., Igarashi, C. and El Abed, A. 2004. Mapping *Posidonia* meadows on Messioua Bank off Zarzis, Tunisia, using multi-beam sonar and GIS. *In* GIS/spatial analyses in fisheries and aquatic sciences. Nishida, T., Kaiola, P. J., Hollingworth, C. E. (eds.), pp. 83–100, Fishery-Aquatic GIS Research Group, Kawagoe, Saitama, Japan.

Komatsu, T., Igarashi, C., Tatsukawa, K., Nakaoka, M., Hiraishi, T. and Taira, A. 2002a. Mapping of seagrass and seaweed beds using hydro-acoustic methods. Fish. Sci. 68: sup. I, 580–583.

Komatsu, T., Igarashi, C., Tatsukawa, K., Sultana, S., Matsuoka, Y. and Harada, S. 2003a. Use of multi-beam sonar to map seagrass beds in Otsuchi Bay, on the Sanriku Coast of Japan. Aquat. Living Resor. 16: 223–230.

Komatsu, T., Ishida, K., Iizumi, H., Okamoto, M. and Belsher, T. 2001. Utilization of ALOS data for mapping coastal ecosystem and managing fisheries activity, *In* Proceedings 1st ALOS PI Workshop, March 28–March 30, 2001, pp. 384–386, NASDA, Tokyo.

Komatsu, T., Sagawa, T., Sawayama, S., Tanoue, H., Mohri, A. and Sakanishi, Y. 2012. Mapping is a key for sustainable development of coastal waters: Examples of seagrass beds and aquaculture facilities in Japan with use of ALOS images. *In* Sustainable development. Ghenai, C. C. (ed.), pp. 145–160, ISBN 979-953-307-649-1. In Tech Publishing Co., Rijeka, Croatia.

Komatsu, T., Tatsukawa, K., Ishida, K., Igarashi, C., Sultana, S., Takahashi, M. and Matsuoka, Y. 2002b. Development of methods mapping coastal zone along Sanriku Coast using satellite imagery and acoustic survey. *In* Conserving our coastal environment: Man and the ocean. UNU-ORI-Iwate Symposium Marine Ecology and Environment, pp. 33–47, United Nations University, Tokyo.

Komatsu, T., Mikami, A., Sultana, S., Ishida, K., Hiraishi, T. and Tatsukawa, K. 2003b. Hydro-acoustic methods as a practical tool for cartography of seagrass beds. Otsuchi Mar. Sci. 28: 72–79.

Lathrop, R. G. Montesano, P. and Haag, S. 2006. A multi-scale segmentation approach to mapping seagrass habitats using. Photogram. Eng. Remote Sens. 72: 665–675.

Lee, Z., Hu, C., Shang, S., Du, K., Lewis, M., Arnone, R. and Brewin, R. 2013. Penetration of UV-visible solar radiation in the global oceans: Insights from ocean color remote sensing. J Geophys. Res: Ocean. 118: 4241–4255.

Lefèvre, J. R., Meinesz, A. and Gloux, B. 1984. Premières données sur

la comparaison de trois méthôdes de cartographie des biocénoses marines. Rapp. P.-V. Réun. Comm. Int. Explor. Sci. Mer Mediterr. 29: 209–211.

Lurton, X. 2002. An introduction to underwater acoustics: Principles and applications. Springer, Berlin.

Lyons, A. P. and Abraham, D. A. 1999. Statistical characterization of high-frequency shallow-water seafloor backscatter. J. Acoust. Soc. Am. 106: 1307–1315.

Lyzenga, D. R. 1978. Passive remote-sensing techniques for mapping water depth and bottom features. Appl. Optics 17: 379–383.

Lyzenga, D. R. 1981. Remote sensing of bottom reflectance and water attenuation parameters in shallow water using aircraft and Landsat data. Int. J. Remote Sens. 10: 53–69.

Ma, Z. and Redmond, R. L. 1995. Tau coefficients for accuracy assessment of classification of remote sensing data. Photogram. Eng. Remote Sens 61: 435–439.

McKenzie, L. J. 2003. Guidelines for the rapid assessment and mapping of tropical seagrass habitats. QFS, NFC, Cairns, 46 pp. https://www.researchgate.net/profile/Len_McKenzie/publication/268423725_Guidelines_for_the_rapid_assessment_of_seagrass_habitats_in_the_western_Pacific/links/573aa8e308aea45ee83f976b/Guidelines-for-the-rapid-assessment-of-seagrass-habitats-in-the-western-Pacific.pdf

Meinesz, A. 1997. Balisage de la limite inférieure de l'herbier de *Posidonia oceanica* en rade de Villefranche-sur-Mer (Alpes-Maritimes, France). Rapp. P.-V. Réun. Comm. Int. Explor. Sci. Mer Mediterr. 24: 143–144.

Meinesz, A. and Laurent, R. 1978. Cartographie et état de la limite inférieure de l'herbier de *Posidonia oceanica* dans les Alpes-maritimes (France) —Campagne Poseidon 1976—. Bot. Mar. 21: 513–526.

Meinesz, A., Cuvelier, M. and Laurent, R. 1981. Méthode récentes de cartographie et de surveillance des herviers de Phanérogames marines. Vie Milieu 31: 27–34.

Mellors, J. E. 1991. An evaluation of a rapid visual technique for estimating seagrass biomass. Aquat. Bot. 42(1): 67–73.

Miller, I. R., Jonker, M. and Coleman, G. 2009. Crown-of-thorns starfish and coral surveys using the manta tow and SCUBA search techniques. Australian Institute of Marine Science. Townsville, Australia.

Mumby, P. J. and Edwards, A. 2000. Water column correction techniques. *In* Remote sensing handbook for tropical coastal management. Edwards, A. J. (ed.), pp. 121–128, UNESCO, Paris.

Mumby, P. J. and Green, E. P. 2000. Field survey: building the link between image and reality. *In* Remote sensing handbook for tropical coastal management. Edwards, A. J. (ed.), pp. 57–66, UNESCO, Paris.

Mumby, P. J., Clark, C. D., Green, E. P. and Edwards, A. J. 1998. Benefits of water column correction and contextual editing for mapping coral reefs. Int. J. Remote Sens. 19: 203–210.

Mumby, P. J., Edwards, A. J., Green, E. P., Anderson, C. W., Ellis, A. C. and Clark, C. D. 1997a. A visual assessment technique for estimating seagrass standing crop. Aquatic Conservation: Mar. Fresh. Ecosys. 7(3): 239–251.

Mumby, P. J., Green, E. P., Edwards, A. J. and Clark, C. D. 1997b. Measurement of seagrass standing crop using satellite and digital airborne remote sensing. Mar. Ecol. Prog. Ser. 159: 51–60.

Mumby, P. J., Green, E. P., Edwards, A. J. and Clark, C. D. 1999. The cost-effectiveness of remote sensing for tropical coastal resources assessment and management. J. Environ. Manag. 55: 157–166.

Naylor, R. L., Goldburg, R. J., Primavera, J. H., Kautsky, N., Beveridge, M. C., Clay, J., Folke, C., Lubchenco, J., Mooney H. and Troell, M. 2000. Effect of aquaculture on world fish supplies. Nature 405(6790): 1017–1024.

Newton, R. S. and Stefanon, A. 1975. Application of side scan sonar in marine biology. Mar. Biol. 31: 287–291.

Norris, J. G., Wyllie-Echeverria, S., Mumford, T., Bauley, A. and Turner, T. 1997. Estimating basal area coverage of subtidal seagrass beds using underwater videography. Aquat. Bot. 58: 269–287.

Onishi, Y., Mohri, Y., Tuji A., Ohgi, K., Yamaguchi, A. and Imai, I. 2014. The seagrass *Zostera marina* harbors growth-inhibiting bacteria against the toxic dinoflagellate *Alexandrium tamarense*. Fish. Sci. 80: 353–362.

Parnum, I. M. 2007. Benthic habitat mapping using multibeam sonar system. PhD Thesis, Department of Imaging and Applied Physics, Curtin University of Technology, Perth, Australia.

Parnum, I. M. and Gavrilov, A. N. 2011. High-frequency multibeam echo-sounder measurements of seafloor backscatter in shallow water: Part 1-Data acquisition and processing. Underw. Technol. 30: 3–12.

Pasqualini, V., Pergent-Martini, C., Clabaut, P. and Pergent, G. 1998. Mapping of *Posidonia oceanica* using aerial photographs and side scan sonar: Application off Island of Corsica (France). Estuar. Coast. Shelf Sci. 47: 359–367.

Pasqualini, V., Pergent-Martini, C., Pergent, G., Agreil, M., Skoufas, G., Sourbes, L. and Tsirika, A. 2005. Use of SPOT 5 for mapping seagrasses: An application to *Posidonia oceanica*. Remote Sens. Environ. 94: 39–45.

Phinn, S., Roelfsema, C., Dekker, A., Brando, V. and Anstee, J. 2008. Mapping seagrass species, cover and biomass in shallow waters: An assessment of satellite multi-spectral and airborne hyper-spectral imaging systems in Moreton Bay (Australia). Remote Sens. Environ. 112: 3413–3425.

Ramos, M. A. and Ramos-Espla, A. 1989. Utilization of acoustic methods in the cartography of the *Posidonia oceanica* bed in the bay of Alicante (SE, Spain). Posidonia Newsletter 2: 17–19.

Riegl, B., Moyer, R. P., Morris, L., Virnstein, R. and Dodge, R. E. 2005. Determination of the distribution of shallow-water seagrass and drift algae communities with acoustic seafloor discrimination. Rev. Biol. Trop. 53: 165–174.

Rey, J. and Diaz del Rio, V. 1989. Cartographia de los fondos marinos de la Bachia de Palma (Baleares, Espana): Distribution de las praderas vegetales y sedimentos superficiales. *In* International Workshop on Posidonia beds 2 GIS. Boudouresque, C.-F., Meinesz, A., Fresi, E. and Gravez, V. (eds.), pp. 29–41, Posidonie Press, Marseille.

Robbins, B. D. and Bell, S. S. 1994.. Seagrass landscapes: A terrestrial approach to the marine subtidal environment. Trend. Ecol Evol. 9: 301–304.

Roelfsema, C., Kovacs, E. M., Saunders, M. I., Phinn, S., Lyons, M. and Maxwell, P. 2013. Challenges of remote sensing for quantifying changes in large complex seagrass environments. Estuar. Coast. Shelf Sci. 133: 161–171.

Sabol, B. M., Melton, R. E., Chamberlain, R., Doering, P. and Haunert,

K. 2002. Evaluation of a digital echo sounder system for detection of submersed aquatic vegetation. Estuar. 25: 133–141.

Sagawa, T., Mikami, A., Komatsu, T., Kosaka, N., Kosako, A., Miyazaki, S. and Takahashi, M. 2008. Mapping seagrass beds using IKONOS satellite image and side scan sonar measurements: A Japanese case study. Int. J. Remote Sens. 29: 281–291.

Sagawa, T., Boisnier, E. Komatsu, T., Ben Mustapha, K., Hattour, A., Kosaka, N. and Miyazaki, S. 2010. Using bottom surface reflectance to map coastal marine areas: A new application method for Lyzenga's model. Int. J. Remote Sens. 31: 3051–3064.

Tanaka, M. and Tanaka, K. 1985. On the estimation of the abundance of seaweed in coastal area I, estimation by echosounder. Fish. Civil Eng. 21: 17–23. (in Japanese).

Tanre, D., Deroo, C., Duhaut, P., Herman, M., Morcrette, J. J., Perbos, J. and Deschamps, P. Y. 1990. Description of a computer code to simulate the satellite signal in the solar spectrum: 5S code. Int. J. Remote Sens. 11: 659–668.

Taylor, M. 2005. IKONOS planetary reflectance and mean solar exoatmospheric irradiance, IKONOS planetary reflectance QSOL Rev.1. Available online at: http://www.geoeye.com/products/imagery/ikonos/spectral.htm (accessed 15 January 2016).

Tecchiato, S., Collins, L., Parnum, I. M. and Stevens, A. 2015. The influence of geomorphology and sedimentary processes on benthic habitat distribution and littoral sediment dynamics: Geraldton, Western Australia. Mar. Geol. 359: 148–162.

Traganos, D. and Reinartz, P. 2018. Mapping Mediterranean seagrasses with Sentinel-2 imagery. Mar. Pollut. Bull. 134: 197–209.

Urbański, J. A., Mazur, A. and Janas, U. 2010. Object-oriented classification of Quickbird data for mapping seagrass spatial structure. Int. J. Oceanogr. Hydrobiol. 38: 27–43.

USGS. 2014. Using the USGS Landsat 8 Product. Available online at: http://landsat.usgs.gov/Landsat8_Using_Product.php (accessed 15 December 2015).

Vermote, E., Tanre, D., Deuze, J. L., Herman, M. and Morcrette, J. J. 1997. Second simulation of the satellite signal in the solar spectrum, 6S: An overview, IEEE T. Geosci. Remote Sens. 35: 675–686.

Ward, L. G., Kemp, W. M. and Boyton, W. R. 1984. The influence of waves and seagrass communities on suspended particulates in an estuarine embayment. Mar. Geol. 59: 85–103.

Wilson, P. S. and Dunton, K. H. 2009. Laboratory investigation of the acoustic response of seagrass tissue in the frequency band 0.5–2.5 kHz. J. Acoust. Soc. Am. 125: 1951–1959.

Xiaohe, Z., Liang, Z., Jixian, Z. and Huiyong, S. 2014. An object-oriented classification method of high resolution imagery based on improved AdaTree. IOP Conference Series: Earth and Environmental Science, 17, 012212. doi:10.1088/1755-1315/17/1/012212